

PCCP

Accepted Manuscript



This article can be cited before page numbers have been issued, to do this please use: X. Lu, K. Shao, B. Fu, X. Wang and D. H. Zhang, *Phys. Chem. Chem. Phys.*, 2018, DOI: 10.1039/C8CP04045A.



This is an Accepted Manuscript, which has been through the Royal Society of Chemistry peer review process and has been accepted for publication.

Accepted Manuscripts are published online shortly after acceptance, before technical editing, formatting and proof reading. Using this free service, authors can make their results available to the community, in citable form, before we publish the edited article. We will replace this Accepted Manuscript with the edited and formatted Advance Article as soon as it is available.

You can find more information about Accepted Manuscripts in the [author guidelines](#).

Please note that technical editing may introduce minor changes to the text and/or graphics, which may alter content. The journal's standard [Terms & Conditions](#) and the ethical guidelines, outlined in our [author and reviewer resource centre](#), still apply. In no event shall the Royal Society of Chemistry be held responsible for any errors or omissions in this Accepted Manuscript or any consequences arising from the use of any information it contains.

An accurate full-dimensional potential energy surface and quasiclassical trajectory dynamics of the H + H₂O₂ two-channel reaction

New Article Online
DOI: 10.1039/C8CP04045A

Xiaoxiao Lu^{1,2}, Kejie Shao², Bina Fu^{2,*}, Xingan Wang^{1,*}, Dong H. Zhang^{2,*}

¹*Department of Chemical Physics, University of
Science and Technology of China, Hefei 230026, China*

²*State Key Laboratory of Molecular Reaction Dynamics
and Center for Theoretical and Computational Chemistry,
Dalian Institute of Chemical Physics, Chinese Academy of Sciences,
Dalian 116023, People's Republic of China*

Abstract

We report a new full-dimensional potential energy surface (PES) of the H + H₂O₂ reaction, covering both H₂ + HO₂ and OH + H₂O product channels. The PES was constructed using the recently proposed fundamental invariant neural network (FI-NN) approach based on roughly 110000 *ab initio* energy points by high level UCCSD(T)-F12/aug-cc-pVTZ calculations. The small fitting error (5.7 meV) and various tests imply a faithful representation of the discrete *ab initio* data over a large configuration space. Extensive quasiclassical trajectory (QCT) calculations were carried out on the new PES at the collision energy (E_c) of 15.0 kcal/mol. The reaction yields dominantly OH+H₂O, because of the lower reaction barrier and much larger reaction exothermicity (~71 kcal/mol) for this channel. Due to the exit barrier of both reaction channels, the most available energy is partitioned into the translational motion of the products. Considerable vibrational excitations of the product H₂O are seen, in particular for the symmetric stretch and bending modes. The angular distributions show predominantly backward scattering, which is consistent with the direct rebound mechanism.

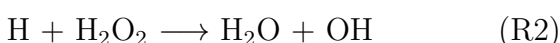
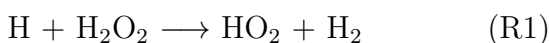
*Authors to whom correspondence should be addressed. Electronic addresses: bina@dicp.ac.cn
xawang@ustc.edu.cn and zhangdh@dicp.ac.cn.

I. INTRODUCTION

View Article Online
DOI: 10.1039/C8CP04045A

Due to its eminent role in fundamental combustion chemistry and hydrocarbon/fuel combustion, the H₂/O₂ combustion system has been extensively investigated[1–6]. The oxidation of H₂ has a major contribution to the later stages of hydrocarbon oxidation. However, significant discrepancies between theoretical modeling and experiments for the H₂/O₂ combustion mechanism exists and much more related work to the H₂/O₂ system is essential to improve this situation[3–5].

In this work, we investigate the following two reactions, which play a critical role in the H₂/O₂ combustion[6–16],



In addition, Reaction (R2) is also an important reaction in the atmosphere, the environment, and the interstellar medium[17, 18]. In the regions of high density of oxygen, this reaction is an important step to the formation of H₂O and OH[19].

Low-temperature measurements of the rate coefficients of reactions (R1) and (R2) indicate large differences in the absolute magnitude of total rate coefficient and in the relative rate branching ratio, probably due to the same reactants involved in the two reactions[20–24]. Theoretically, Truhlar and coworkers investigated the two reactions by performing extensive electronic structure calculations[25]. The rate coefficients were also calculated by canonical variational transition state theory with multidimensional tunneling[26–28], where two possible sets of recommended rate coefficients based on different electronic structure calculations were given to match the evaluated experimental values. Recently, Lamberts *et al* used instanton theory to compute rate coefficients for reactions (R1) and (R2) at low temperatures down to 50K[19]. The electronic structure calculations were mainly based on density functional theory (DFT), with barrier heights additionally determined by unrestricted single-reference and multireference coupled-cluster calculations. It was found that the single-reference calculations result in nearly the same barrier as the multi-reference calculations for the two reactions, indicating the multi-reference character is not important in those regions. By comparing coupled cluster barrier heights to those obtained with DFT, they suggested the two reactions have to be described by using two different DFT methods.

Due to the large computational efforts of coupled cluster calculations, the DFT calculations were further used to investigate the reaction on water surfaces.

To the best of our knowledge, there is no global full-dimensional *ab initio* potential energy surface (PES) and dynamics calculations for the H + H₂O₂ multichannel reaction. In this article, we report an accurate full-dimensional PES for the title reaction based on high-level coupled cluster calculations. The PES was constructed by fundamental invariant-neural network (FI-NN) fitting[29] to roughly 114000 data points, computed at the explicitly correlated unrestricted coupled cluster single, double, and perturbative triple levels with the augmented correlation corrected valence triple-zeta basis set (UCCSD(T)-F12b/AVTZ)[30]. Extensive quasiclassical trajectory calculations were carried out on the new PES, to investigate the detailed dynamics information for the title multichannel reaction.

This paper is organized as follows. Section II gives the detailed fitting procedures and the properties of the PES, as well as the QCT calculations. In Section III, we present the dynamics information obtained by the QCT calculations on the new PES. A summary of the current results and conclusions is given in Section IV.

II. POTENTIAL ENERGY SURFACE

We constructed a new global PES of the H+H₂O₂ reaction, leading to both H₂O+OH and HO₂+H₂ product channels based on high-level *ab initio* and fitting methods.

The energy points used in the fitting were selected properly based on direct dynamics simulations and further QCT calculations using the preliminary PESs. The initial dataset consists of roughly 40 000 energy points with the configurations taken from direct dynamics calculations using the unrestricted B3LYP/6-31+g* level of theory. For these calculations, a total of about 300 trajectories were run from the reagents H + H₂O₂ at the collision energies of 15.0 kcal/mol. Additional roughly 300 trajectories were run initiated from the transition states leading to two different product channels. Starting from the first PES based on the initial 40 000 UCCSD(T)-F12b/AVTZ energies, more data points were added iteratively by doing QCT calculations on those preliminary PESs. In addition, more data points around the reaction pathways leading to two product channels were calculated and added to the data set.

Considering the possible multi-reference character in some regions of the PES, further T1

diagnostic calculations were carried out to check the reliability and monitor the quality of coupled cluster calculations[31]. A small number of energy points with T1 diagnostic values larger than 0.05 was discarded. A total of roughly 114000 UCCSD(T)-F12b/aug-cc-pVTZ energy points were computed using MOLPRO 2012.1[32] and included in the fundamental invariant-neural network (FI-NN) fitting procedure.

The neural network (NN) method is a general fitting method, which is extremely flexible and in principle it can be used to fit any shape of function with very high accuracy[33]. For a chemical system with identical atoms, the potential energy should be invariant with respect to the permutations of identical atoms. Hence, the permutation symmetry is an important factor which needs to be considered in the construction of PESs. Since the NN functions are not symmetric with respect to the permutation of identical atoms, the energy is not exactly continuous at a configuration with two or more equal internuclear distances, which may introduce some errors in QCT calculations but can produce accurate results in quantum dynamics calculations[34, 35].

The following three fitting approaches are good candidates for the construction of high-dimensional PESs with permutational symmetry. The first is the permutationally invariant polynomial (PIP) fitting approach developed by Bowman and coworkers[36–38], which has been applied to construct a large number of accurate permutationally invariant polyatomic PESs[36–42]. The PIP method uses primary and secondary invariants as the fitting basis to generate permutation invariant polynomials. Another mathematically equivalent method based on the symmetrized monomials was also developed by Bowman and coworkers[43]. Second, this PIP approach further inspired Guo and coworkers, who proposed the PIP-NN fitting approach[44, 45]. The PIP-NN approach employs a set of PIPs instead of pairwise distances as input vector in the neural network, which can automatically guarantee the permutational symmetry. The input PIPs include all the polynomials truncated by a given degree. However, the number of polynomials increases considerably with the degree bound. It is unrealistic to include all the invariant polynomials with the highest degree bound of secondary invariants in the input vector. The number of polynomials can be reduced with a lower degree bound, but a large number of secondary polynomials have to be discarded. Thus, recently a more flexible NN approach using the fundamental invariants (FIs) as the input vector was proposed by Zhang and coworkers to construct the PESs with permutational symmetry[29, 46]. Different from the polynomials in PIP and the polynomials in the PIP-

NN method, FI minimizes the size of input invariants and contains the least number of invariants, which can generate all the invariant polynomials. FI-NN can efficiently reduce the evaluation time of potential energy compared to the corresponding PIP-NN PESs, in particular for larger molecular systems with more identical atoms.

Here, we used the FI-NN method to fit the global PES of the title reaction based on high level UCCSD(T)-F12b/aug-cc-pVTZ energy points, where the permutation symmetry of all three hydrogen atoms and two oxygen atoms is taken into account.

The FIs can be calculated by King's algorithm[47] implemented in the computer algebra system called Singular[48]. For the H_3O_2 molecular system, three H atoms are labeled as atoms 1,2,3 and two O atoms are labeled as atoms 4 and 5. The pairwise internuclear distances $(r_{12}, r_{13}, r_{14}, r_{15}, r_{23}, r_{24}, r_{25}, r_{34}, r_{35}, r_{45})$ is expressed as $(x_1, x_2, x_3, \dots, x_8, x_9, x_{10})$.

The FIs calculated are as follows,

View Article Online
DOI: 10.1039/C8CP04045A

$$\begin{aligned}
 p(1) &= x_3 + x_4 + x_6 + x_7 + x_8 + x_9 \\
 p(2) &= x_1 + x_2 + x_5 \\
 p(3) &= x_3^2 + x_4^2 + x_6^2 + x_7^2 + x_8^2 + x_9^2 \\
 p(4) &= x_3x_4 + x_6x_7 + x_8x_9 \\
 p(5) &= x_3x_6 + x_4x_7 + x_3x_8 + x_6x_8 + x_4x_9 + x_7x_9 \\
 p(6) &= x_1x_3 + x_2x_3 + x_1x_4 + x_2x_4 + x_1x_6 + x_5x_6 + x_1x_7 + x_5x_7 + x_2x_8 + x_5x_8 + x_2x_9 + x_5x_9 \\
 p(7) &= x_1^2 + x_2^2 + x_5^2 \\
 p(8) &= x_3^3 + x_4^3 + x_6^3 + x_7^3 + x_8^3 + x_9^3 \\
 p(9) &= x_3^2x_4 + x_3x_4^2 + x_6^2x_7 + x_6x_7^2 + x_8^2x_9 + x_8x_9^2 \\
 p(10) &= x_3^2x_6 + x_3x_6^2 + x_4^2x_7 + x_4x_7^2 + x_3^2x_8 + x_6^2x_8 + x_3x_8^2 + x_6x_8^2 + x_4^2x_9 + x_7^2x_9 + x_4x_9^2 + x_7x_9^2 \\
 p(11) &= x_1x_3^2 + x_2x_3^2 + x_1x_4^2 + x_2x_4^2 + x_1x_6^2 + x_5x_6^2 + x_1x_7^2 + x_5x_7^2 + x_2x_8^2 + x_5x_8^2 + x_2x_9^2 + x_5x_9^2 \\
 p(12) &= x_1x_3x_4 + x_2x_3x_4 + x_1x_6x_7 + x_5x_6x_7 + x_2x_8x_9 + x_5x_8x_9 \\
 p(13) &= x_1x_3x_6 + x_1x_4x_7 + x_2x_3x_8 + x_5x_6x_8 + x_2x_4x_9 + x_5x_7x_9 \\
 p(14) &= x_1^2x_3 + x_2^2x_3 + x_1^2x_4 + x_2^2x_4 + x_1^2x_6 + x_5^2x_6 + x_1^2x_7 + x_5^2x_7 + x_2^2x_8 + x_5^2x_8 + x_2^2x_9 + x_5^2x_9 \\
 p(15) &= x_1^3 + x_2^3 + x_5^3 \\
 p(16) &= x_3^4 + x_4^4 + x_6^4 + x_7^4 + x_8^4 + x_9^4 \\
 p(17) &= x_3^3x_4 + x_3x_4^3 + x_6^3x_7 + x_6x_7^3 + x_8^3x_9 + x_8x_9^3 \\
 p(18) &= x_3^3x_6 + x_3x_6^3 + x_4^3x_7 + x_4x_7^3 + x_3^3x_8 + x_6^3x_8 + x_3x_8^3 + x_6x_8^3 + x_4^3x_9 + x_7^3x_9 + x_4x_9^3 + x_7x_9^3 \\
 p(19) &= x_1x_3^3 + x_2x_3^3 + x_1x_4^3 + x_2x_4^3 + x_1x_6^3 + x_5x_6^3 + x_1x_7^3 + x_5x_7^3 + x_2x_8^3 + x_5x_8^3 + x_2x_9^3 + x_5x_9^3 \\
 p(20) &= x_1x_3^2x_6 + x_1x_3x_6^2 + x_1x_4^2x_7 + x_1x_4x_7^2 + x_2x_3^2x_8 + x_5x_6^2x_8 + x_2x_3x_8^2 + \\
 &\quad x_5x_6x_8^2 + x_2x_4^2x_9 + x_5x_7^2x_9 + x_2x_4x_9^2 + x_5x_7x_9^2 \\
 p(21) &= x_1^2x_3^2 + x_2^2x_3^2 + x_1^2x_4^2 + x_2^2x_4^2 + x_1^2x_6^2 + x_5^2x_6^2 + \\
 &\quad x_1^2x_7^2 + x_5^2x_7^2 + x_2^2x_8^2 + x_5^2x_8^2 + x_2^2x_9^2 + x_5^2x_9^2 \\
 p(22) &= x_1^2x_3x_6 + x_1^2x_4x_7 + x_2^2x_3x_8 + x_5^2x_6x_8 + x_2^2x_4x_9 + x_5^2x_7x_9 \\
 p(23) &= x_3^5 + x_4^5 + x_6^5 + x_7^5 + x_8^5 + x_9^5 \\
 p(24) &= x_1x_3^4 + x_2x_3^4 + x_1x_4^4 + x_2x_4^4 + x_1x_6^4 + x_5x_6^4 + x_1x_7^4 + x_5x_7^4 + x_2x_8^4 + x_5x_8^4 + x_2x_9^4 + x_5x_9^4 \\
 p(25) &= x_3^6 + x_4^6 + x_6^6 + x_7^6 + x_8^6 + x_9^6 \\
 p(26) &= x_{10}
 \end{aligned}$$

Overall, there is a total of 26 fundamental invariants with the maximum degree of 6 for the H₃O₂ molecular system, which is significantly smaller than the corresponding PIPs in the PIP-NN approach. Li *et al* uses 138 PIPs with a specific maximum order of 4 in calculating the PIP-NN PES of the OH+H₂O → H₂O+OH exchange reaction[49]. For these FIs, the set of internuclear distances (x_1, \dots, x_{10}) is further displaced by Morse-like variables in all internuclear distances [$y_i = \exp(-x_i/\lambda)$; where $\lambda = 1.0 \text{ \AA}$]. The fit used the 26 invariants as the input vector of neural network.

The feed forward NN with two hidden layers connecting the input and output layer is recorded as I-J-K-1 NN. It has I nodes in the input layer, namely the 26 invariants, and one node in the output layer corresponding to potential energy value of the input molecular configuration. There are J and K neurons in the two hidden layer, respectively.

The output of j^{th} neuron in the first hidden layer is

$$y_j^1 = f^1 \left(b_j^1 + \sum_{i=1}^I (w_{j,i}^1 \times x_i) \right), \quad j = 1, 2, \dots, J \quad (1)$$

and the output of k^{th} neuron in the second hidden layer is

$$y_k^2 = f^2 \left(b_k^2 + \sum_{j=1}^J (w_{k,j}^2 \times y_j^1) \right). \quad k = 1, 2, \dots, K \quad (2)$$

Therefore, the final result is given by

$$y = b_1^3 + \sum_{k=1}^K (w_{1,k}^3 \times y_k^2), \quad (3)$$

where $x_i (i = 1, \dots, I)$ denote the internuclear distances of a molecular configuration. The i^{th} and j^{th} neurons of $(l - 1)^{th}$ and l^{th} layers, respectively, were connected by the weights $w_{j,i}^l$. The threshold of the j^{th} neuron of l^{th} layer is determined by the biases b_j^l , and the transfer functions f^1 and f^2 are taken as hyperbolic tangent functions.

During the NN fitting procedure, we have to perform many tests by using different number of neurons for the two hidden layers based on a specific set of data points, in order to get the smallest fitting error, mainly because the structure of NN strongly influences the quality of fit. For a specific NN structure, the weights and biases in Eq. (1)-(3) can be updated through proper NN training using the Levenberg-Marquardt algorithm[50].

The root mean square error (RMSE)

$$\text{RMSE} = \sqrt{\frac{1}{n} \sum_{i=1}^n (\text{E}_{\text{fit}} - \text{E}_{\text{ab initio}})^2} \quad (4)$$

is used to measure the fitting error. Furthermore, we used the "early stopping" method[51] to improve the fitting quality. The entire data set was divided into the training and validation sets, and the training procedure was inhibited when the over fitting occurs.

Based on the above fitting scheme, the final FI-NN PES was fitted using the total of 26 fundamental invariants as the input vector of NN and the 26-50-60-1 NN structure, resulting in a small RMSE of 5.7 meV or 0.13 kcal/mol for energies up to 190 kcal/mol relative to the global minimum ($\text{OH} + \text{H}_2\text{O}$) of the PES. The final PES is well converged with respect to the fitting errors and dynamic features. The treatment of the long-range regions of a PES is important[52], when the dynamics is particularly focused on very low collision energies, i.e., low temperature collisions. Those systems usually features with quite low reaction barriers. Since the barrier heights for the title reactive system are roughly 9.8 kcal/mol and 6.2 kcal/mol for the two product pathways, the reaction dynamics at collision energies higher or slightly lower than the barrier heights can be interesting. We did not pay much attention to accurately describe the long-range interaction for this system, due to the relatively high collision energy. The PES is available from the corresponding authors upon request.

TABLE I: Relative Energy (kcal/mol), Zero Point Energy (kcal/mol), and Harmonic Frequencies (cm^{-1}) for the $\text{H} + \text{H}_2\text{O}_2$ System

Species	Energy ^a	ZPE ^b	Frequencies ^c
$\text{H} + \text{H}_2\text{O}_2$	0.00(0.00)	16.66 (16.67)	393, 918, 1320, 1430, 3789, 3801 [381, 914, 1330, 1437, 3798, 3798]
$\text{H}_2 + \text{HO}_2$	-15.75(-15.66)	15.25 (15.23)	4408; 1149, 1441, 3671 [4401; 1148, 1442, 3660]
$\text{OH} + \text{H}_2\text{O}$	-71.09(-71.07)	18.87 (18.82)	3764; 1648, 3841, 3945 [3741; 1648, 3834, 3944]
TS1	9.80(9.81)	15.33 (14.96)	i2389, 412, 532, 779, 960, 1239, 1472, 1561, 3762 [i2355, 398, 452, 687, 980, 1245, 1412, 1536, 3752]
TS2	6.25(6.27)	17.03 (16.91)	i1191, 231, 318, 412, 782, 1218, 1363, 3763, 3825 [i1285, 159, 331, 435, 786, 1213, 1319, 3786, 3794]

^a The fitted energies on the FI-NN PES are relative to $\text{H} + \text{H}_2\text{O}_2$. The values in the parentheses are from UCCSD(T)-F12b/aug-cc-pVTZ calculations.

The PES fits well to the *ab initio* energies as can be seen from Fig. 1, which shows the fitting errors of all data points as a function of their corresponding *ab initio* energies. The minimum energy paths for $\text{H}+\text{H}_2\text{O}_2 \rightarrow \text{H}_2+\text{HO}_2$ and $\text{H}+\text{H}_2\text{O}_2 \rightarrow \text{OH}+\text{H}_2\text{O}$, which were determined by the Quadratic Steepest Descent method[53] on the PES, are depicted in Fig. 2(a) and Fig. 2(b), respectively, together with those results calculated by the UCCSD(T)-F12b/aug-cc-pVTZ level of theory. The reaction coordinate s is defined to be the signed distance along the reaction path of steepest descent through mass-scaled Cartesian coordinates from the saddle point ($s=0$) to the reactants (at which $s=-\infty$) and the path from this saddle point to the products (at which $s=+\infty$). Obviously, smooth reaction path curves were obtained on the PES for the two product channels, which are both activated and exoenergetic reactions. The collision of H and H_2O_2 either proceeds via a barrier (TS1) of 9.8 kcal/mol, resulting in the H_2+HO_2 product, or proceeds via a barrier (TS2) of 6.25 kcal/mol, leading to the formation of $\text{OH}+\text{H}_2\text{O}$ with a large exoergicity of roughly 71 kcal/mol. Furthermore, excellent agreement for energies on the reaction paths is achieved between the PES and UCCSD(T)-F12b/AVTZ values. The maximum fitting error for energy points on the reaction paths is only 0.1 kcal/mol.

A comparison of the geometries and energies of reactant asymptote $\text{H}+\text{H}_2\text{O}_2$, two transition states TS1 and TS2, and two product asymptotes $\text{OH}+\text{H}_2\text{O}$ and $\text{H}_2+\text{H}_2\text{O}$ from the fitted PES and directly from the *ab initio* UCCSD(T)-F12 calculations is given in Fig. 3. As seen from the figure, the PES describes the stationary points with good accuracy, with the maximum deviation of bond length from UCCSD(T)-F12 results of 0.4%, bond angle of %, dihedral angle of 2%, and energy of 0.5%.

The corresponding relative energies to the reagent, vibrational zero-point energies (ZPEs) and harmonic frequencies of stationary points obtained on the FI-NN PES are shown in Table 1, which are also compared with the UCCSD(T)-F12b/AVTZ calculations. The comparisons made for the energies obtained from the current FI-NN PES and UCCSD(T)-F12b/AVTZ calculations indicate very good agreement among them, with the maximum fitting error of 0.09 kcal/mol, as shown in Fig. 3 and Table I. In addition, the ZPEs as well as the harmonic frequencies for various stationary points obtained on the PES agree quite well with the direct *ab initio* calculations.

Contour plot of the FI-NN PES for $\text{H}+\text{H}_2\text{O}_2 \rightarrow \text{H}_2+\text{HO}_2$ as a function of R_{HH} and R_{OH} , together with that for $\text{H}+\text{H}_2\text{O}_2 \rightarrow \text{OH}+\text{H}_2\text{O}$ as a function of R_{OH} and R_{OO} is shown in Fig.

4(a) and Fig. 4(b), respectively, with other degrees of freedom fixed at the corresponding transition states (TS1/TS2). The coordinates R_{HH} and R_{OH} of Reaction (R1), and R_{OH} and R_{OO} of Reaction (R2) were indicated by blue fonts in the geometries of TS1 and TS2 in Fig. 3, respectively. Overall, the L-shape reaction paths for the two reaction channels are quite smooth. In addition, we plot the two-dimensional (2D) cuts for the above contours, in comparison with the UCCSD(T)/AVTZ results. The 2D cuts as functions of R_{HH} and R_{OH} , with other coordinates fixed at TS1 are displayed in Fig. 5. The corresponding 2D cuts with other coordinates fixed at TS2 are shown in Fig. 6. Obviously, the *ab initio* energies calculated with UCCSD(T)-F12b/AVTZ (black circles) are reproduced well on the FI-NN PES for these curves. The maximum fitting error for energy points on the 2D cuts is only 0.2 kcal/mol. All of these results indicate that the current FI-NN PES for the title reaction is sufficiently accurate to be used in dynamics calculations.

III. QUASICLASSICAL TRAJECTORY CALCULATIONS

There are two reaction pathways starting from $H + H_2O_2$, ending with the formation of $H_2 + HO_2$ via TS1 and the formation of $OH + H_2O$ via TS2. The $H + H_2O_2$ reaction can, in principle, evolve via the two reaction pathways to the formation of two sets of products.

Standard QCT calculations[39–42, 54–56] for the $H+H_2O_2$ reaction were carried out at the collision energy of 15.0 kcal/mol on the new FI-NN PES, with H_2O_2 initially in the ground rovibrational state. Initial coordinates and momenta of H_2O_2 were obtained by randomly sampling the normal coordinates and momenta. Adjustments were then made to the momenta to enforce zero angular momentum of H_2O_2 . The initial distance of the H atom from the center of mass of H_2O_2 was $\sqrt{x^2 + b^2}$, where b is the impact parameter and x was set to 11.0 Bohr. The maximum impact parameter (b_{max}) was set to 8.5 Bohr. The orientation of H_2O_2 was randomly sampled and b was selected randomly from the distribution $b_{max}\sqrt{r}$, where r is a random number uniformly distributed from 0 to 1. Roughly 12000000 trajectories were performed using the Velocity-Verlet integration algorithm with a time step of 0.073 fs for a maximum time of 50 ps. The trajectories were terminated when the distance of two fragments became larger than 13.0 Bohr. Almost all trajectories conserved energy to within 0.05 kcal/mol, confirming the smoothness and accuracy of the PES. As a result, the trajectories ended up either going into one of the two product channels or returning to the

reactants.

In this study, we further investigate how these distributions can be affected by the ZPE issue arising from the QCT calculations. The violation of ZPE constraint is an important issue that should be considered in the QCT calculations. Here, we investigate how final distributions can be affected by the ZPE issue arising from the QCT calculations, in which three treatments were employed to analyze the final products as was done in previous work. For a specific product channel, the ZPE constrained analysis considered trajectories in which each of the products has at least the corresponding ZPE. The soft ZPE constrained analysis is employed for those trajectories in which the sum of the vibrational energies of products is not less than the sum of the corresponding ZPEs. We consider all the trajectories with no ZPE constraint. And finally, we employed the 1GB approach[57–59] to analyze the final product distributions when necessary.

By analyzing all the reactive trajectories, we got the reactive branching percentages of the two product channels at $E_c = 15.0$ kcal/mol, namely the $\text{H}_2 + \text{HO}_2$ channel and the $\text{OH} + \text{H}_2\text{O}$ channel, which is roughly 1:9, 1:16, 1:13 with the soft ZPE constraint, ZPE constraint and 1GB treatment. The $\text{OH} + \text{H}_2\text{O}$ channel is the dominant reaction pathway, due to the lower barrier height and much larger exoergicity compared to the $\text{H}_2 + \text{HO}_2$ channel.

A. THE $\text{H}_2 + \text{HO}_2$ CHANNEL

The detailed dynamics information for $\text{H} + \text{H}_2\text{O}_2 \rightarrow \text{H}_2 + \text{HO}_2$ was obtained on the FI-NN PES by analyzing trajectories. Fig. 7(a) shows the center of mass (CM) translational energy distributions of $\text{H}_2 + \text{HO}_2$, $P(E_T)$, using different ZPE treatments. Significant differences were seen among the three translational energy distributions from three batches of trajectories, indicating the remarkable ZPE violation of the product vibrational energy of either H_2 or HO_2 from many trajectories. Due to the exit barrier of this product channel, most of the available energy (~ 32.2 kcal/mol) is partitioned into the translational motion of the products.

The result with non-ZPE constraint gives a distribution up to the energy of 42 kcal/mol, indicating that a large fraction of either product is formed with ZPE violations. The translational energy distribution with the soft-ZPE constraint has a peak around 23 kcal/mol, with the value of $P(E_T)$ up to the available energy of about 32 kcal/mol. The averaged transla-

tional energy release for this channel is about 23 kcal/mol, corresponding to a large fraction (0.71) of the total available energy (32.2 kcal/mol). This indicates most of the available energy in this channel is deposited into the relative movement of the H₂+HO₂ products, and a very small portion of energy is partitioned into the internal degrees of freedom of the products. The distribution with the ZPE constraint has the similar shape, but with a shift of roughly 2 kcal/mol compared to the soft-ZPE constraint. The translational energy distribution with the 1GB treatment is broader than the corresponding soft ZPE and ZPE constraint results.

The center of mass angular distributions of the H₂ product calculated by different ZPE constraints on the FI-NN PES are all similar, thus the statistically more robust results with soft ZPE constraint are shown in Fig. 7(b). Obviously, the H₂ product is mainly scattered in the backward hemisphere relative to the incoming H atom direction, with relatively small sideways scattering signals, which is consistent with the main rebound mechanism for this H atom abstraction reaction. Contributions from sideways scattering are mainly due to the emission of the H₂ molecule from the collision intermediate nearly orthogonal to the plane of the H-O-O atoms. Two animations of backward scattering and sideways scattering for this reaction channel are given in the supporting information.

A 3D polar plot for the product translational energy and angular distributions for the H₂+HO₂ channel is shown in Fig. 8. We can see that the predominant backward scattering peak mainly resides in the high kinetic energy region, indicating the high excitation of the translational movement/low internal excitation of the products.

We find the H₂ product is formed dominantly in the ground vibrational state (v=0) from trajectory calculations. The vibrational state populations of v=0 and v=1 are 76% and 24 and 96% and 4%, respectively, with the soft ZPE constraint and 1GB treatment. The rovibrational state distribution of H₂ shown in Fig. 9 indicates low rotational excitation of H₂. The peak of the rotational distributions of OH with the soft ZPE constraint is at *j*=3. The rotational excitations with the 1GB treatment are higher than those with the soft ZPE constraint, with the peak of distribution changing from *j*=6 for v=0 to *j*=3 for v=1.

The mode-specific HO₂(ν_1, ν_2, ν_3) vibrational distributions were computed to further investigate the HO₂ + H₂ product channel, where ν_1, ν_2 and ν_3 corresponds to the O-H stretching, bending and O-O stretching modes of HO₂. As indicated in Table I, the harmonic frequencies for the O-H stretching, bending and O-O stretching are 1148 cm⁻¹, 1441

cm^{-1} , 3671 cm^{-1} , respectively. The normal-mode analysis of HO_2 based on the total vibrational energy of the vibrational states was carried out using the same approach as described elsewhere[40, 42, 58, 60]. To determine the harmonic actions of HO_2 , the normal mode analysis was preceded by removing the rotation of the molecule and maintain the orientation of the optimized geometry of the HO_2 molecule for which the normal mode analysis was being performed. A projection of the displacement and momentum matrices onto the normal mode space was then obtained for the computation of the potential and kinetic energies for each normal mode.

Figure 10(a) shows the mode-specific vibrational distributions of HO_2 , using the soft ZPE and 1GB treatments. The distributions obtained from the two treatments are similar. The HO_2 product is formed with low vibrational excitations, where the ground vibrational state occupies nearly 50% of product. The O-H stretch vibrational states (100) and (200) account for roughly 25% and 10% of total populations, respectively. The bending excitation is limited to the quantum number 1, where the (010) and (110) states accounts for 7% and 3% of total populations. We see very little excitation of the O-O stretch, since the population of the first overtone (001) is already less than 1%. All the vibrational states shown here correspond to about 99.4% of the total HO_2 vibrational populations, implying very few higher excited states are open, and their contributions are very small. The rotational energy distributions of HO_2 with soft ZPE and 1GB treatments are shown in Fig. 10(b), with its peak at around 2.0 kcal/mol. The two distributions are quite similar and narrow, which drops to zero at around 7 kcal/mol.

These distributions support that both H_2 and HO_2 products are not highly rovibrationally excited, and most of the total available energy available is partitioned into the translational movement.

B. THE OH + H_2O CHANNEL

Due to the lower barrier height and much larger exoergicity, the $\text{H}+\text{H}_2\text{O}_2$ reaction yields much more $\text{OH} + \text{H}_2\text{O}$, compared to H_2+HO_2 . We display the center of mass (CM) translational energy distribution $P(E_T)$ of $\text{OH} + \text{H}_2\text{O}$ in Fig. 11(a). The results with non-ZPE, soft ZPE and hard ZPE constraints are similar, implying the ZPE effects are not important for this product channel, probably due to the large total available energy (83.88 kcal/mol). The

View Article Online
DOI: 10.1039/C8CP04045A

$P(E_T)$ has a peak around 52 kcal/mol, with the distribution up to the energy of about 80.0 kcal/mol. The averaged translational energy release for this channel is about 51 kcal/mol, indicating a quite large fraction (0.61) of the total available energy (83.88 kcal/mol) is released as translational energy for this channel. As seen from Fig. 11(b), the angular distribution of the H_2O product shows exclusively backward scattering relative to the direction of the incoming H atom, consistent with the direct rebound mechanism for the formation of H_2O+OH .

A 3D polar plot for the product translational energy and angular distributions for this reaction channel is shown in Fig. 12, which exhibits a predominant backward scattering peak in the high translational energy region, but nearly no sideways and forward scattering signals. Analysis of trajectories reveals that the reaction process is fast, with the attack of one oxygen atom of H_2O_2 by the incoming H atom, and the direct breakage of O-O bond followed by the rebound of H_2O . One animation of backward scattering for this reaction channel is given in the supporting information.

Although the most available energies are released as the translational movement of products, there are still substantial energies than can be partitioned into the internal energy of products, due to the large exothermicity for this channel. We also calculated the final rotational and vibrational state distributions of OH and H_2O .

Figure 13 shows the rovibrational state distributions of OH and rotational state distribution of H_2O . The vibrational state populations of OH for $v=0$ and $v=1$ are 81% and 19%, respectively, indicating the product OH is predominantly formed in the ground vibrational state. There are some rotational excitations for OH and H_2O . The rotational state distributions of OH at $v=0$ and $v=1$ are quite similar, which are flat for N_{OH} less than 8, and drop steadily with the further increase of N_{OH} . The rotational state distribution of H_2O rises quickly from $j=0$ with a peak at $j=5$, and then drops steadily and vanishes at $j=25$. The two distributions support that both OH and H_2O products are moderately rotationally excited.

Figure 14 shows the mode-specific vibrational distributions of $H_2O(\nu_1, \nu_2, \nu_3)$, where ν_1, ν_2 and ν_3 corresponds to the symmetric stretch, bending and asymmetric stretch modes of H_2O . We can see the H_2O vibrational state is highly excited, particularly for the symmetric stretch and bending modes. All the vibrational states shown here correspond to about 76.6% of the total H_2O vibrational populations, implying that many higher excited states

are open as well, though their respective population is relatively small. The population of the ground state is 8%, which is slightly smaller than the overtone (100). The largest population is on the first overtone of symmetric stretch (100), and it accounts for about 10.7% of the total populations, compared to 7.5% and 2.7%, 0.8% respectively, for the symmetric stretching overtones (200), (300) and (400). In addition, there are considerable populations for the combined excitations of symmetric stretch and bending/asymmetric stretch. For example, the (210) and (201) states accounts for roughly 4% and 3% of the total populations, respectively. A broad distribution is shown for the bending overtone, with considerable populations for the quantum number up to 6. The excitation of the asymmetric stretch is also seen, with the (001) and (002) overtones populations roughly 2 times and 8 times smaller than the ground state of H₂O.

IV. CONCLUSIONS

To summarize, we constructed a new global PES for the H₃O₂ system based on FI-NN fitting to roughly 110000 *ab initio* energies calculated at the UCCSD(T)-F12b/AVTZ level of theory. A total of 26 fundamental invariants with the maximum degree of 6 was used as the input vector of neural network, which is significantly smaller than the corresponding PIPs at the same degree. It is impractical to include all the PIPs at the maximum degree of 6 in the PIP-NN approach for the H₃O₂ system, but truncated at a specific degree, such as 4. The FI-NN PES is accurate and smooth, based on the small fitting RMSE of 5.7 meV, as well as the well representations of stationary points and reaction paths. Extensive QCT calculations have been performed on the FI-NN PES, and detailed dynamics information, such as the product translational energy, rovibrational state and angular distributions of the H₂ + HO₂ and OH + H₂O product channels are presented and discussed. The H+H₂O₂ → OH+H₂O is the dominant reaction pathway, due to the lower barrier and much larger exothermicity, compared with H+H₂O₂ → H₂+HO₂. The angular distribution of OH displays exclusively backward scattering relative to the direction of the incoming H atom, while that of H₂ shows a predominantly backward scattering peak with some contributions from sideways scattering. These are consistent with the direct rebound mechanism for the two reaction pathways. Those signals from sideways scattering are mainly owing to the emission of H₂ from the collision intermediate nearly orthogonal to the plane of the H-O-O atoms. Because of the

exit barrier of the two reaction pathways, the most of total available energy is partitioned into the translational movement of products. Therefore, the H₂ and HO₂ products of reaction (R1) are rovibrationally cold. In contrast, for reaction (R2), the normal mode analysis reveals substantial vibrational excitations of H₂O, particularly for the symmetric stretch and bending vibrations, whereas OH is formed mainly in the ground vibrational state. Moderate rotational excitations of H₂O and OH are also seen for this reaction pathway. We expect the current work will stimulate a reliable platform of experiment for this important bimolecular reaction in combustion.

View Article Online
DOI: 10.1039/C8CP04045A

-
- [1] M. P. Burke, M. Chaos, F. L. Dryer, and Y. Ju, Combustion and Flame **157**, 618 (2010).
- [2] J. F. Grcar, J. B. Bell, and M. S. Day, Proceedings of the Combustion Institute **32**, 1173 (2009).
- [3] M. J. Davis, R. T. Skodje, and A. S. Tomlin, The Journal of Physical Chemistry A **115**, 1556 (2011).
- [4] S. Bai, D. Zhou, M. J. Davis, and R. T. Skodje, The Journal of Physical Chemistry Letters **6**, 183 (2015).
- [5] A. A. Konnov, Combustion and Flame **152**, 507 (2008).
- [6] G. Dixon-Lewis and D. J. Williams, in *Comprehensive Chemical Kinetics*, edited by C. H. Bamford and C. F. H. Tipper (Elsevier, 1977), vol. 17, pp. 1–248.
- [7] L. Daeyup and H. Simone, International Journal of Chemical Kinetics **30**, 385 (1998).
- [8] J. Warnatz, in *Combustion Chemistry*, edited by W. C. Gardiner (Springer US, New York, NY, 1984), pp. 197–360.
- [9] R. R. Baldwin and L. Mayor, Transactions of the Faraday Society **56**, 80 (1960).
- [10] R. R. Baldwin, L. Mayor, and P. Doran, Transactions of the Faraday Society **56**, 93 (1960).
- [11] R. R. Baldwin and L. Mayor, Transactions of the Faraday Society **56**, 103 (1960).
- [12] R. R. Baldwin, D. Jackson, R. W. Walker, and S. J. Webster, Symposium (International) on Combustion **10**, 423 (1965).
- [13] R. R. Baldwin, D. Jackson, R. W. Walker, and S. J. Webster, Transactions of the Faraday Society **63**, 1665 (1967).
- [14] R. R. Baldwin, D. Jackson, R. W. Walker, and S. J. Webster, Transactions of the Faraday Society **63**, 1665 (1967).

- Society **63**, 1676 (1967).
- [15] R. R. Baldwin, D. Brattan, B. Tunnicliffe, R. W. Walker, and S. J. Webster, Combustion and Flame **15**, 133 (1970).
- [16] R. R. Baldwin and R. W. Walker, Journal of the Chemical Society, Faraday Transactions 1: Physical Chemistry in Condensed Phases **75**, 140 (1979).
- [17] H. M. Cuppen and H. Eric, The Astrophysical Journal **668**, 294 (2007).
- [18] T. Lamberts, X. de Vries, and H. M. Cuppen, Faraday Discussions **168**, 327 (2014).
- [19] T. Lamberts, P. K. Samanta, A. Kohn, and J. Kastner, Physical Chemistry Chemical Physics **18**, 33021 (2016).
- [20] E. A. Albers, K. Hoyermann, H. G. Wagner, and J. Wolfrum, Symposium (International) on Combustion **13**, 81 (1971).
- [21] R. A. Gorse and D. H. Volman, Journal of Photochemistry **3**, 115 (1974).
- [22] R. A. Gorse and D. H. Volman, Journal of Photochemistry **1**, 1 (1972).
- [23] R. B. Klemm, W. A. Payne, and L. J. Stief, in *1st Symposium on Chemical Kinetics Data for the Upper and Lower Atmosphere* (Wiley-Interscience, New York, 1975), pp. 61–72.
- [24] J. Michael, D. Whytock, J. Lee, W. Payne, and L. Stief, The Journal of Chemical Physics **67**, 3533 (1977).
- [25] B. A. Ellingson, D. P. Theis, O. Tishchenko, J. Zheng, and D. G. Truhlar, The Journal of Physical Chemistry A **111**, 13554 (2007).
- [26] D. G. Truhlar and B. C. Garrett, Accounts of Chemical Research **13**, 440 (1980).
- [27] Y. P. Liu, G. C. Lynch, T. N. Truong, D. H. Lu, D. G. Truhlar, and B. C. Garrett, Journal of the American Chemical Society **115**, 2408 (1993).
- [28] D.-h. Lu, T. N. Truong, V. S. Melissas, G. C. Lynch, Y.-P. Liu, B. C. Garrett, R. Steckler, A. D. Isaacson, S. N. Rai, G. C. Hancock, et al., Computer Physics Communications **71**, 235 (1992).
- [29] K. Shao, J. Chen, Z. Zhao, and D. H. Zhang, The Journal of Chemical Physics **145**, 071101 (2016).
- [30] G. Knizia, T. B. Adler, and H.-J. Werner, The Journal of Chemical Physics **130**, 054104 (2009).
- [31] T. J. Lee, Chemical Physics Letters **372**, 362 (2003).
- [32] H.-J. Werner, P. J. Knowles, G. Knizia, F. R. Manby, M. Schütz, P. Celani, W. Györffy,

D. Kats, T. Korona, R. Lindh, et al., *Molpro, version 2015.1, a package of ab initio programs*, View Article Online DOI: 10.1039/C8CP04045A (2015), see <http://www.molpro.net>.

- [33] L. M. Raff, R. Komanduri, M. Hagan, and S. Bukkapatnam, *Neural networks in chemical reaction dynamics* (Oxford University Press, New York, 2012).
- [34] J. Chen, X. Xu, X. Xu, and D. H. Zhang, *The Journal of Chemical Physics* **138**, 154301 (2013).
- [35] J. Chen, X. Xu, X. Xu, and D. H. Zhang, *The Journal of Chemical Physics* **138**, 221104 (2013).
- [36] B. J. Braams and J. M. Bowman, *International Reviews in Physical Chemistry* **28**, 577 (2009).
- [37] J. M. Bowman, G. Czakó, and B. Fu, *Physical Chemistry Chemical Physics* **13**, 8094 (2011).
- [38] C. Qu, Q. Yu, and J. M. Bowman, *Annual Review of Physical Chemistry* **69**, 151 (2018).
- [39] B. Fu, Y.-C. Han, J. M. Bowman, L. Angelucci, N. Balucani, F. Leonori, and P. Casavecchia, *Proceedings of the National Academy of Sciences* **109**, 9733 (2012).
- [40] B. Fu, Y.-C. Han, J. M. Bowman, F. Leonori, N. Balucani, L. Angelucci, A. Occhiogrosso, R. Petrucci, and P. Casavecchia, *The Journal of Chemical Physics* **137**, 22A532 (2012).
- [41] J. Yang, K. Shao, D. Zhang, Q. Shuai, B. Fu, D. H. Zhang, and X. Yang, *The Journal of Physical Chemistry Letters* **5**, 3106 (2014).
- [42] K. Shao, B. Fu, and D. H. Zhang, *Physical Chemistry Chemical Physics* **17**, 24098 (2015).
- [43] Z. Xie and J. M. Bowman, *Journal of Chemical Theory and Computation* **6**, 26 (2010).
- [44] B. Jiang and H. Guo, *The Journal of Chemical Physics* **139**, 054112 (2013).
- [45] J. Li, B. Jiang, and H. Guo, *The Journal of Chemical Physics* **139**, 204103 (2013).
- [46] B. Fu and D. H. Zhang, *Journal of Chemical Theory and Computation* **14**, 2289 (2018).
- [47] S. A. King, *Journal of Symbolic Computation* **48**, 101 (2013).
- [48] W. Decker, G.-M. Greuel, G. Pfister, and H. Schönemann, *SINGULAR 4-1-1 — A computer algebra system for polynomial computations*, <http://www.singular.uni-kl.de> (2018).
- [49] M. Bai, D. Lu, and J. Li, *Physical Chemistry Chemical Physics* **19**, 17718 (2017).
- [50] M. T. Hagan and M. B. Menhaj, *IEEE Transactions on Neural Networks* **5**, 989 (1994).
- [51] W. S. Sarle, in *Proceedings of the 27th Symposium on the Interface of Computing Science and Statistics* (1995), pp. 352–360.
- [52] A. Zanchet, P. del Mazo, A. Aguado, O. Roncero, E. Jimnez, A. Canosa, M. Agndez, and J. Cernicharo, *Phys. Chem. Chem. Phys.* **20**, 5415 (2018), URL <http://dx.doi.org/10.1039/C8CP04045A>.

1039/C7CP05307J.

View Article Online
DOI: 10.1039/C8CP04045A

- [53] J. Sun and K. Ruedenberg, *The Journal of Chemical Physics* **99**, 5269 (1993).
- [54] W. L. Hase, in *Encyclopedia of Computational Chemistry*, edited by N. L. Allinger (Wiley, New York, 2002), vol. 1, pp. 402–407.
- [55] W. L. Hase, in *Encyclopedia of Computational Chemistry*, edited by N. L. Allinger (Wiley, New York, 2002), vol. 1, pp. 399–402.
- [56] Y.-C. Han, P.-Y. Tsai, J. M. Bowman, and K.-C. Lin, *Phys. Chem. Chem. Phys.* **19**, 18628 (2017).
- [57] L. Bonnet, *International Reviews in Physical Chemistry* **32**, 171 (2013).
- [58] G. Czakó and J. M. Bowman, *The Journal of Chemical Physics* **131**, 244302 (2009).
- [59] R. Conte, B. Fu, E. Kamarchik, and J. M. Bowman, *The Journal of Chemical Physics* **139**, 044104 (2013).
- [60] B. Fu, E. Kamarchik, and J. M. Bowman, *The Journal of Chemical Physics* **133**, 164306 (2010).

Acknowledgments

This work was supported by the National Natural Science Foundation of China (Grant nos 21673233, 21722307, 21433009, and 21688102), the Strategic Priority Research Program (Grant No. XDB17000000), and the Youth Innovation Promotion Association (Grant No. 2015143) of the Chinese Academy of Sciences. Bina Fu thanks Xueming Yang and Rex T. Skodje for many useful discussions on this reactive system.

Figure Captions:

View Article Online
DOI: 10.1039/C8CP04045A

Figure 1 The fitting errors for all the data points in the FI-NN PES, as a function of their corresponding *ab initio* energies with respect to H+H₂O₂.

Figure 2 The minimum energy paths for H+H₂O₂ → H₂+HO₂ and H+H₂O₂ → OH+H₂O obtained from the PES (solid lines) and those calculated from UCCSD(T)-F12b/AVTZ theory (symbols). The reaction coordinate is the signed distance along the reaction path from the saddle points.

Figure 3 Optimized geometries (bond lengths in Å, angles in degree) and energies (kcal/mol) of the stationary points on the fitted PESs, compared with the results from the UCCSD(T)-F12b/AVTZ calculations (in parentheses).

Figure 4 (a) Contour plot of H+H₂O₂ → H₂+HO₂ on the FI-NN PES, as functions of R_{HH} and R_{OH} (indicated in Fig. 3), with other degrees of freedom fixed at the transition state. (b) Contour plot of H+H₂O₂ → OH+H₂O, as functions of R_{OH} and R_{OO} (indicated in Fig. 3), with other degrees of freedom fixed at the transition state.

Figure 5 Two-dimensional (2D) cuts for Fig. 4(a) obtained from the PES (solid lines), in comparison with those calculated from UCCSD(T)-F12b/AVTZ theory (symbols).

Figure 6 2D cuts for Fig. 4(b) obtained from the PES (solid lines), in comparison with those calculated from UCCSD(T)-F12b/AVTZ theory (symbols).

Figure 7 (a) Center-of-mass (CM) translational energy distribution of H₂+HO₂ with different ZPE constrains obtained from the QCT calculations. The total available energy is indicated by the black arrow. (b) Angular distribution of H₂ relative to the direction of the incoming H.

Figure 8 3D polar plot for the product translational energy and angular distributions for the H₂+HO₂ channel. The forward direction (0°) corresponds to the direction of the H reagent.

Figure 9 Rovibrational state distribution of H₂.

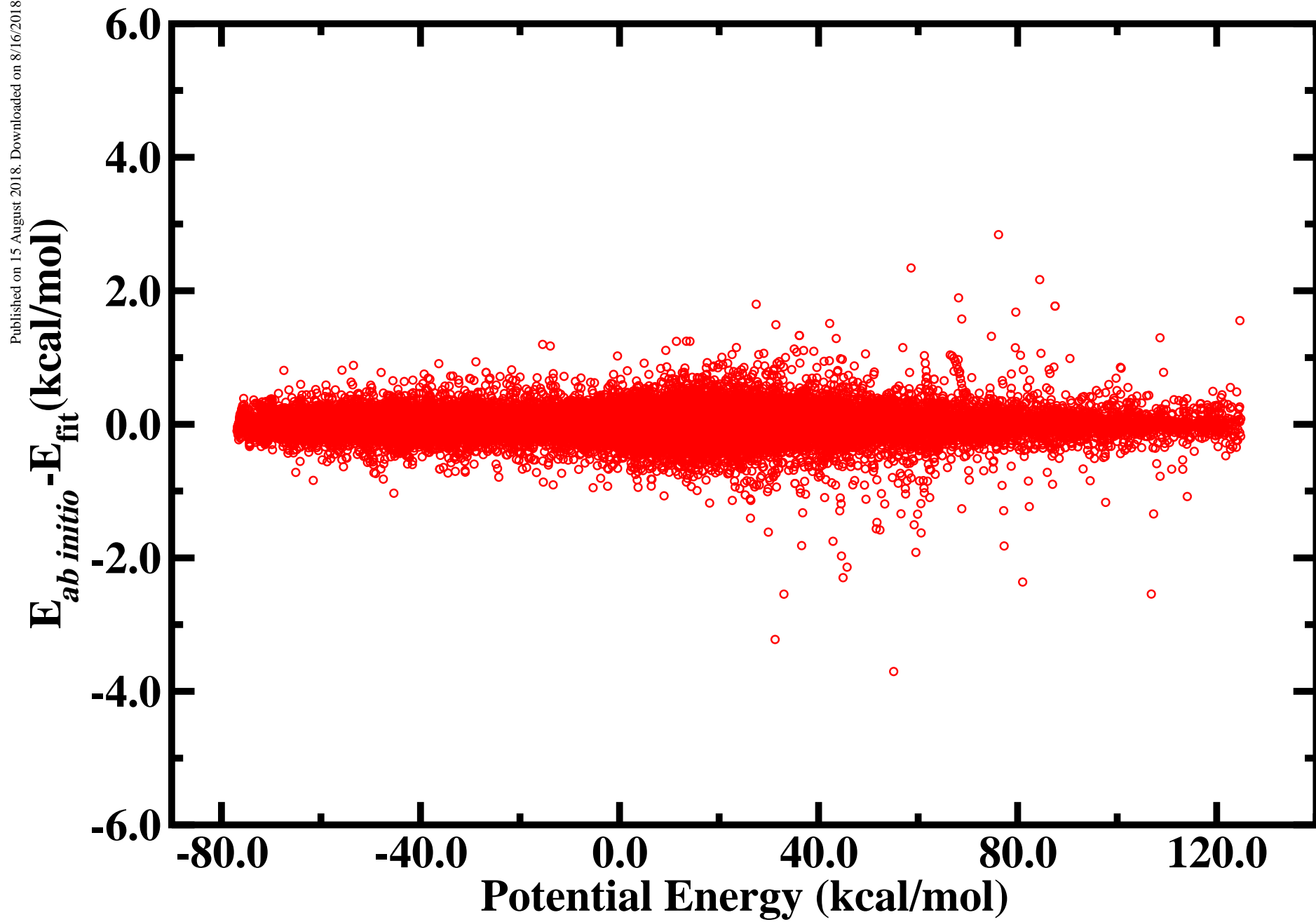
Figure 10 (a) Rotational state distribution of HO₂ for the H₂+HO₂ channel. (b) Mode-specific vibrational state distribution of HO₂.

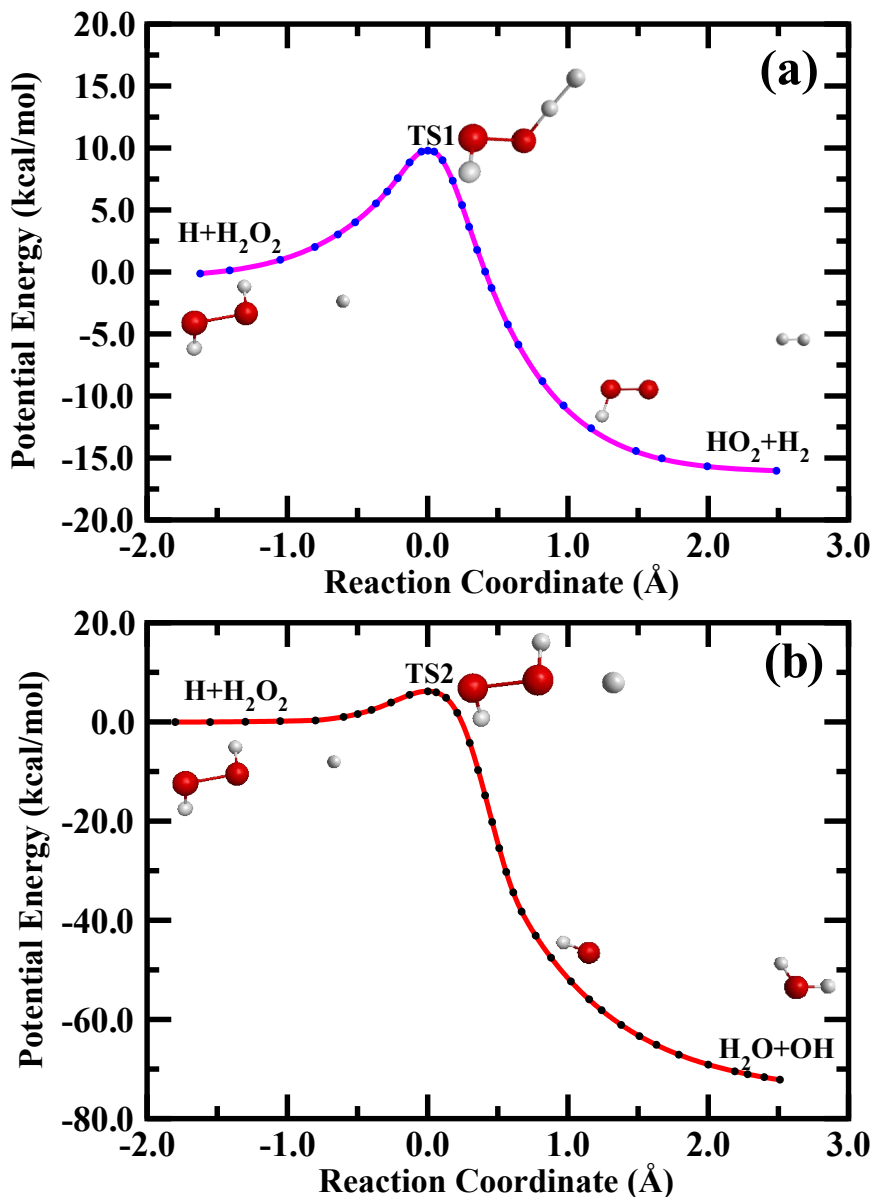
Figure 11 (a) Center-of-mass (CM) translational energy distribution of OH+H₂O with different ZPE constrains obtained from the QCT calculations. The total available energy is indicated by the black arrow. (b) Angular distribution of OH relative to the direction of the incoming H.

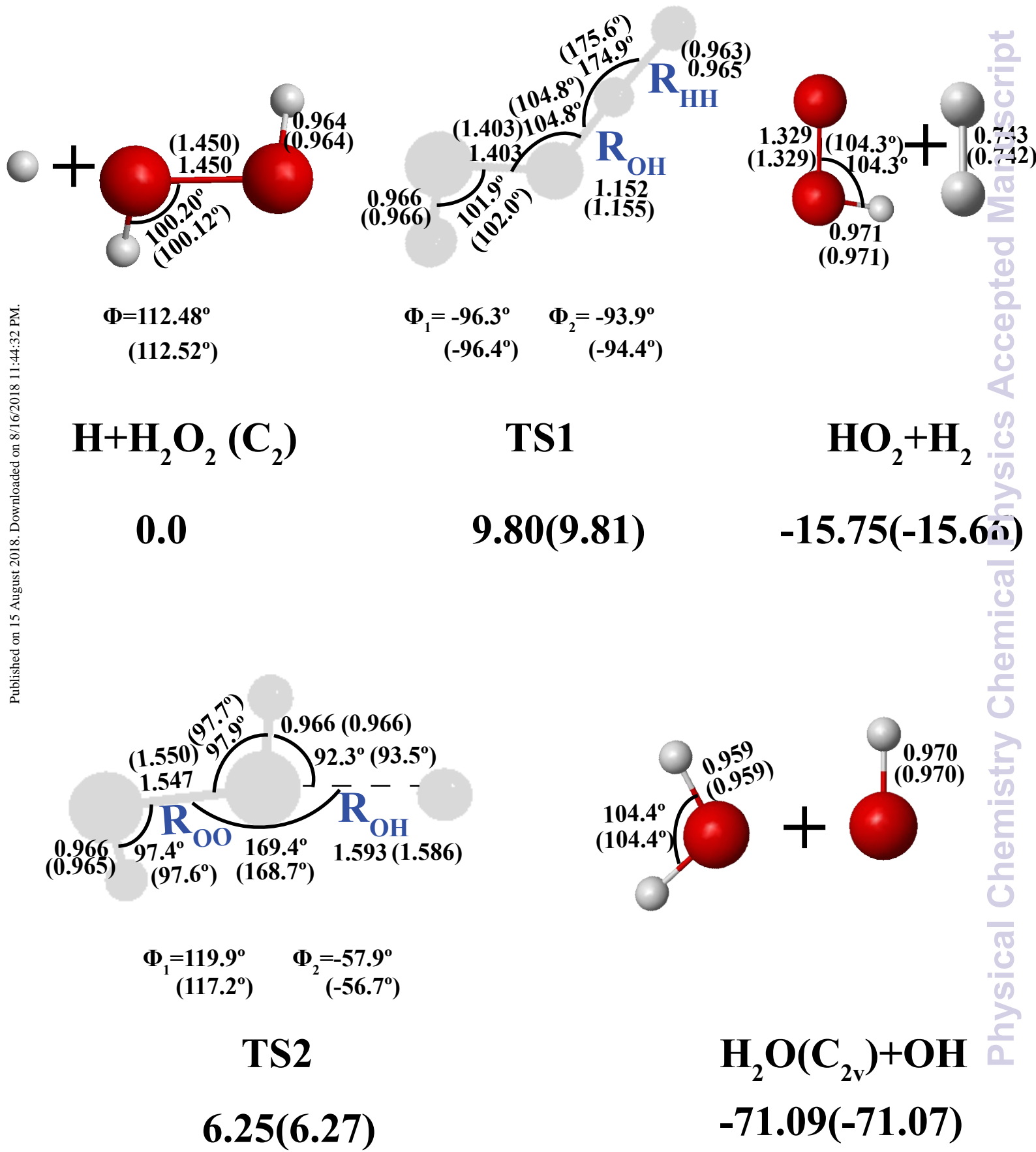
Figure 12 3D polar plot for the product translational energy and angular distributions for the OH+H₂O channel. The forward direction (0°) corresponds to the direction of the H reagent.

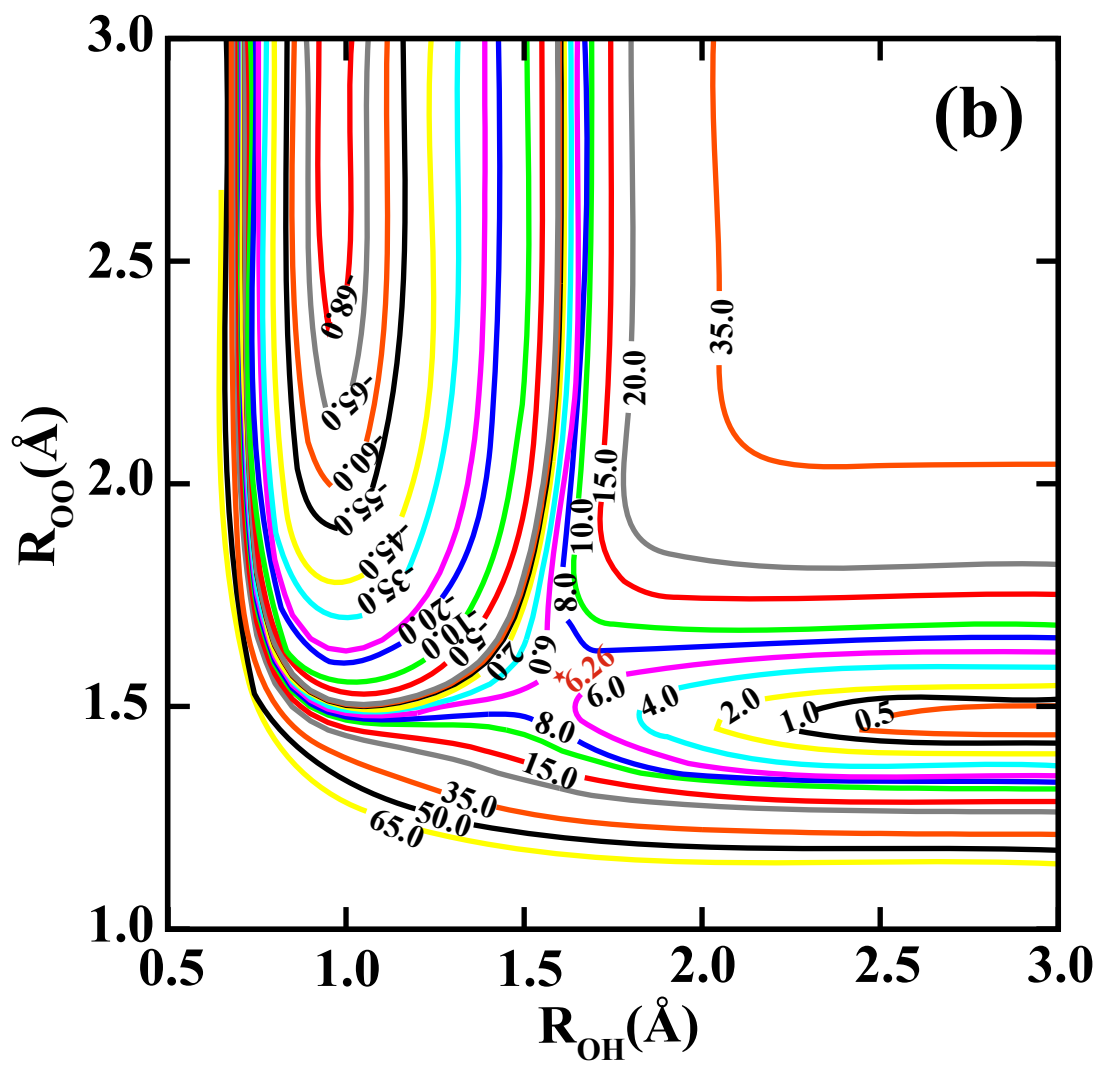
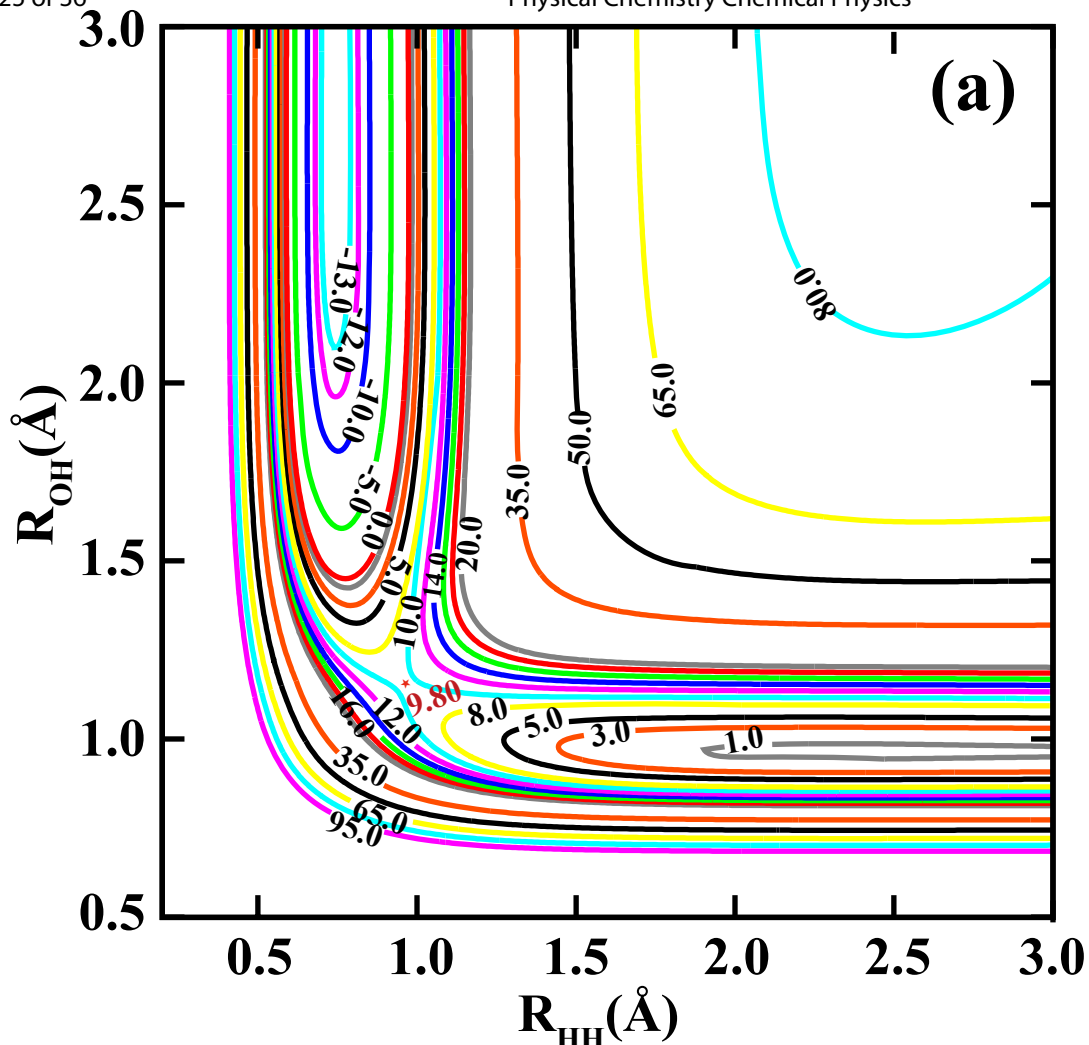
Figure 13 (a) Rovibrational state distribution of OH. (b) Rotational state distribution of H₂O for the OH+H₂O channel.

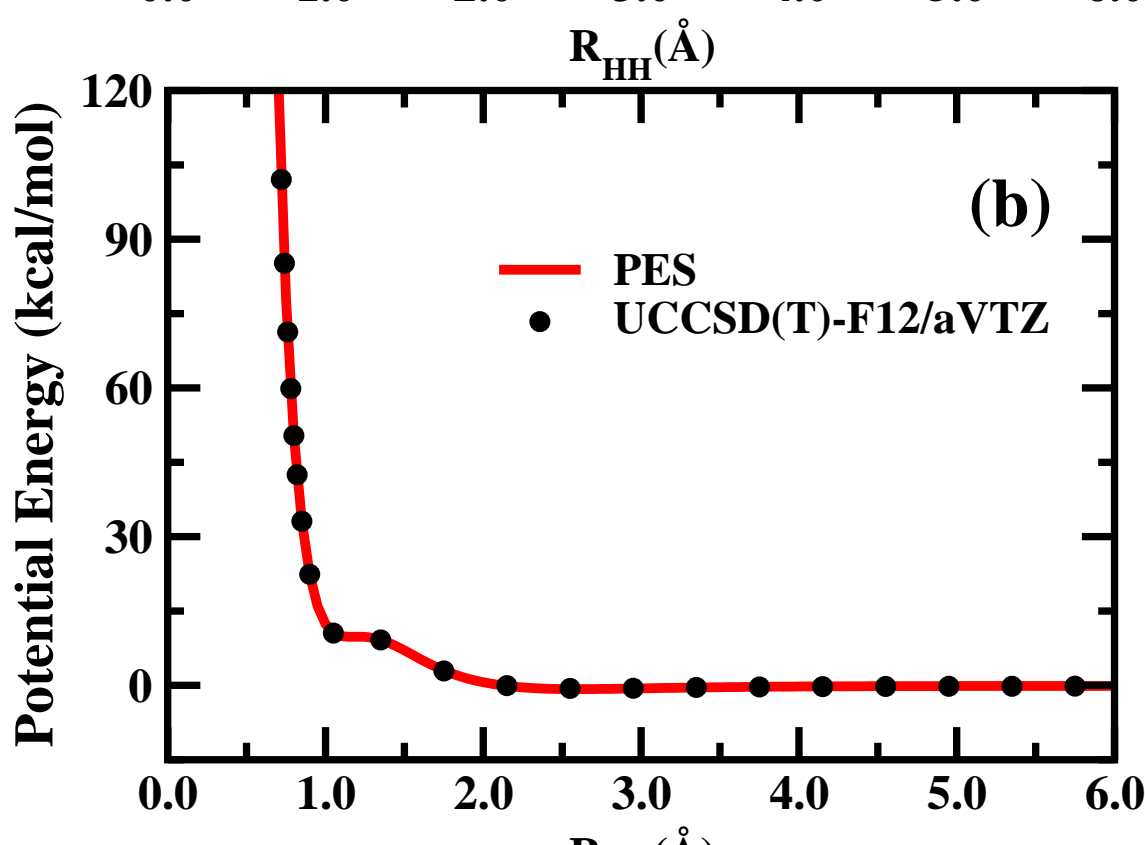
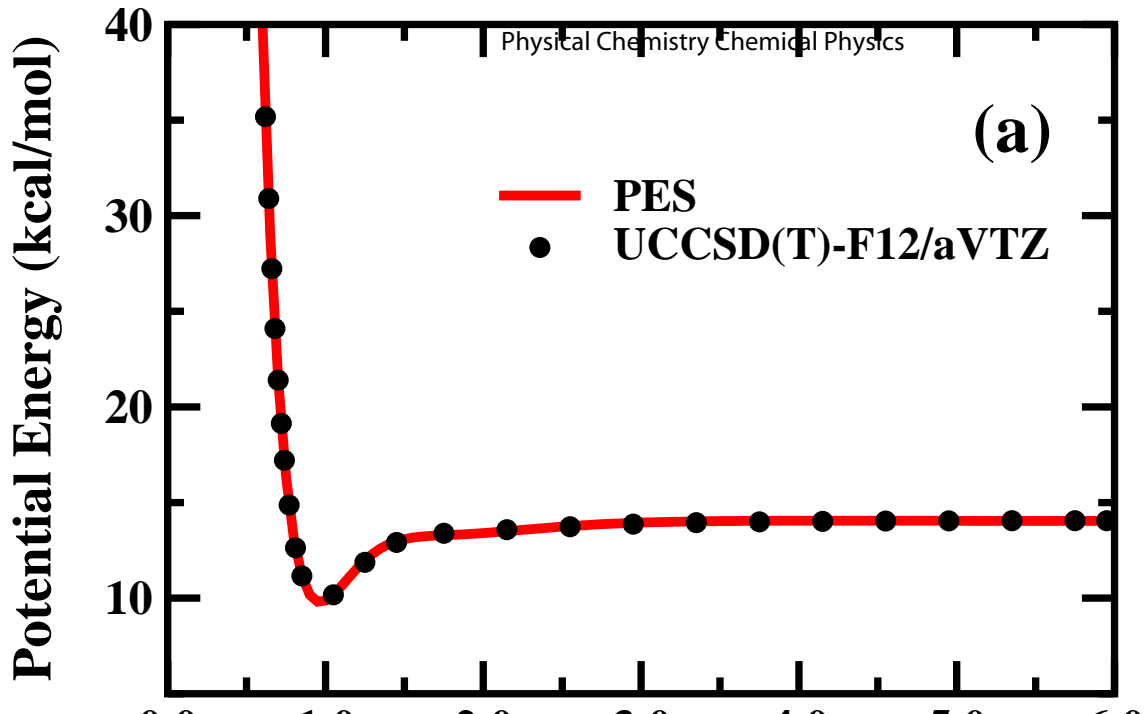
Figure 14 Mode-specific vibrational state distribution of H₂O for the OH+H₂O channel.

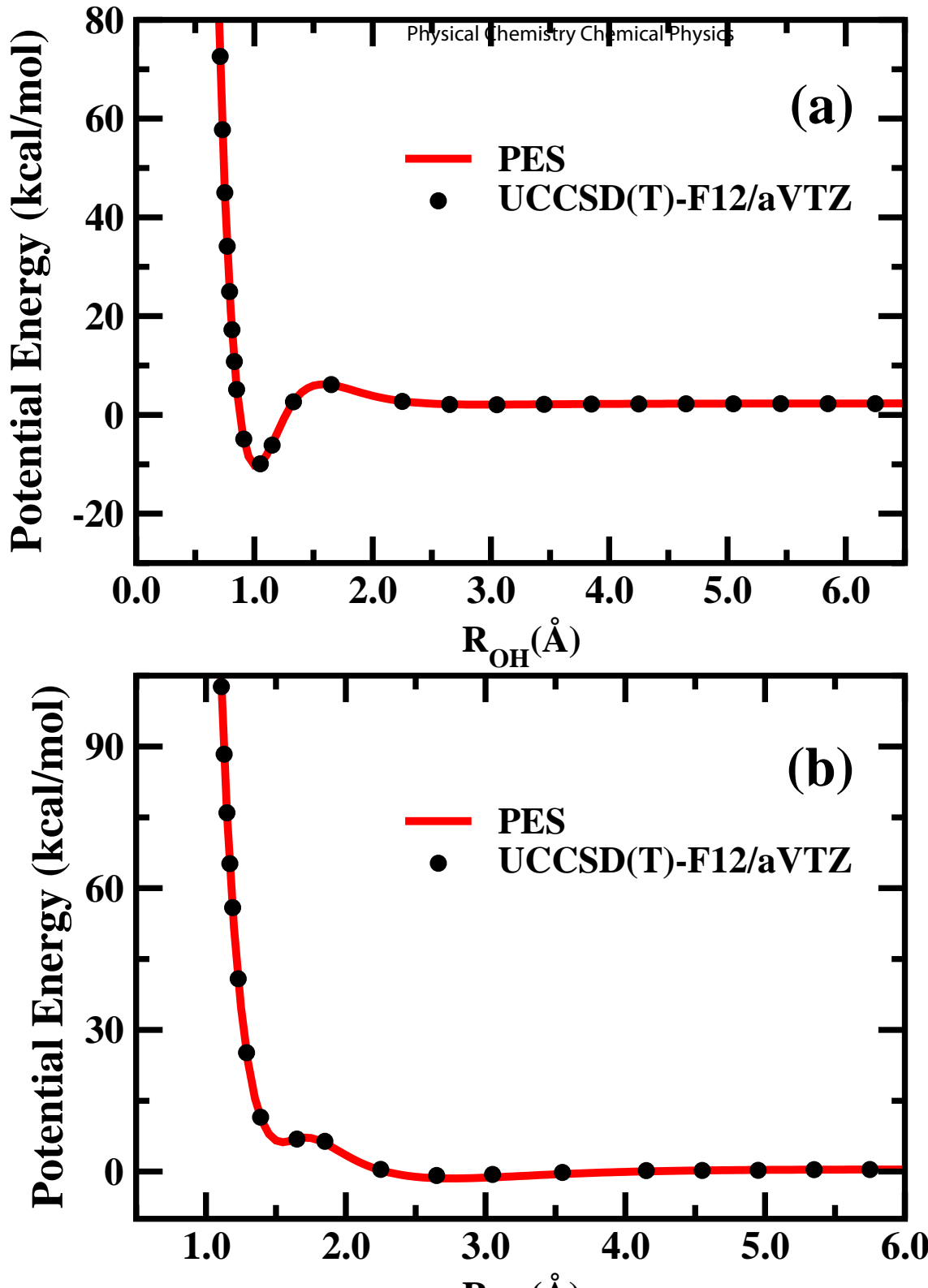


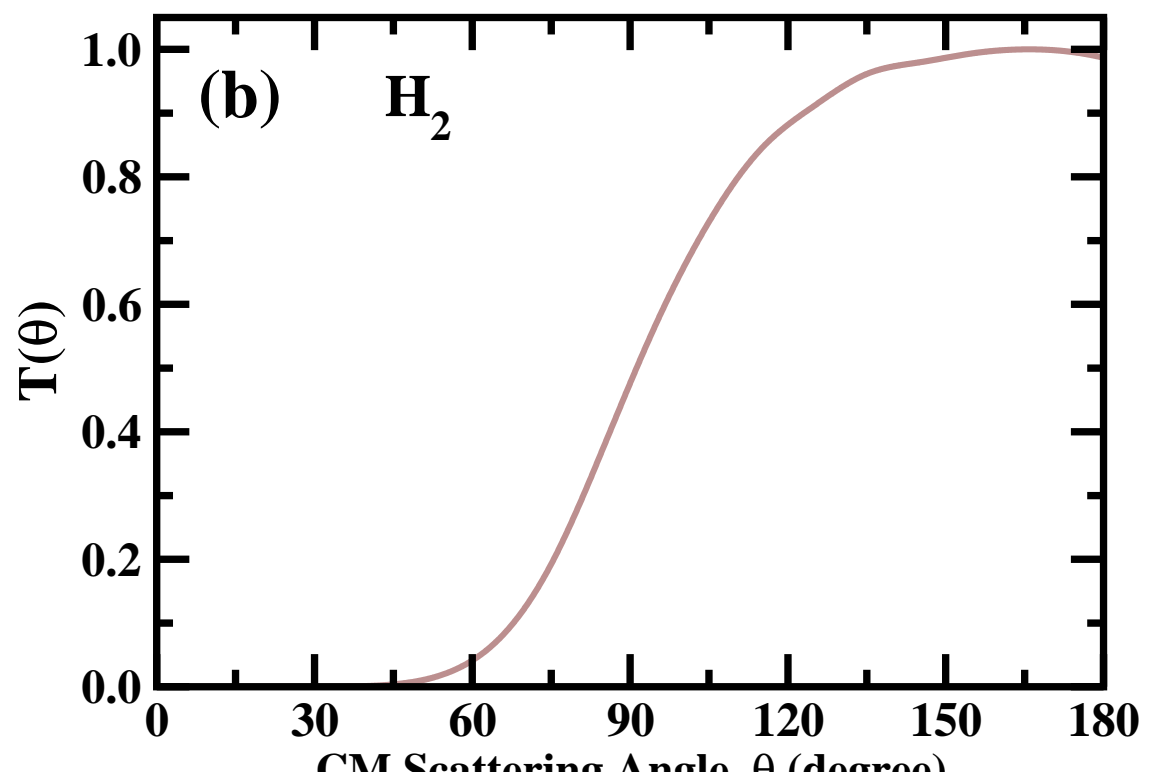
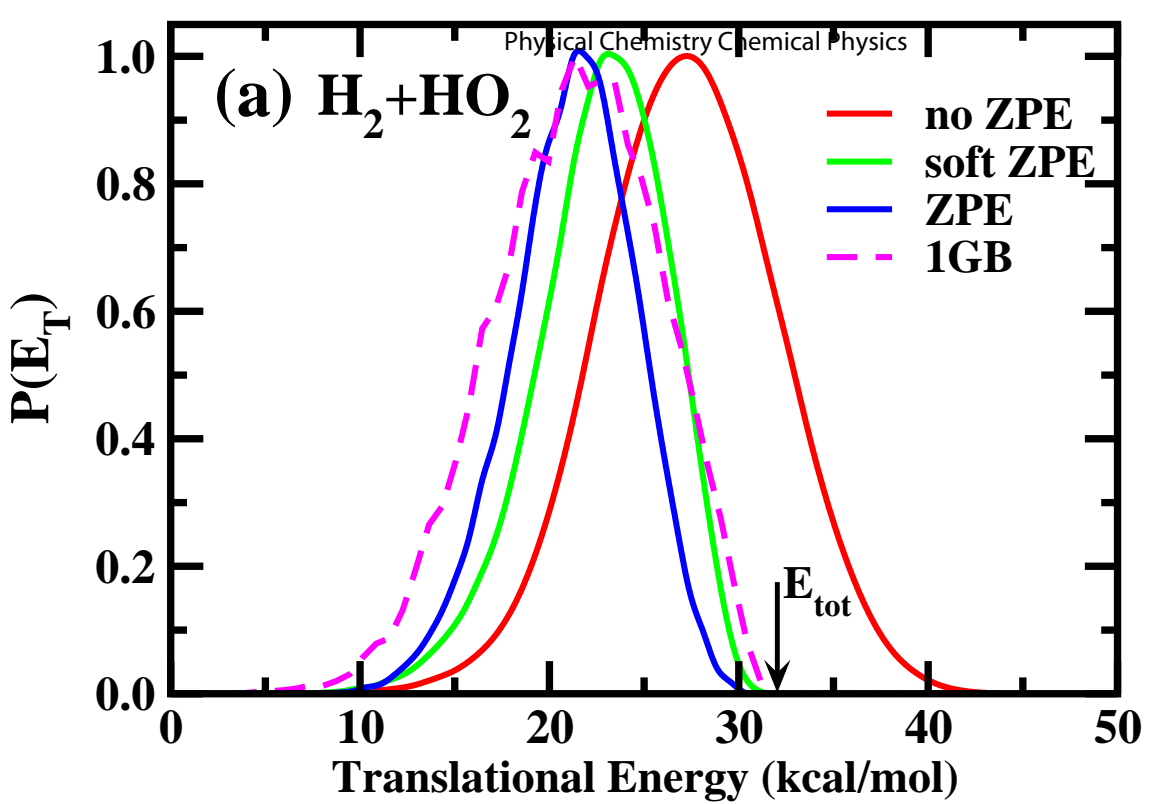


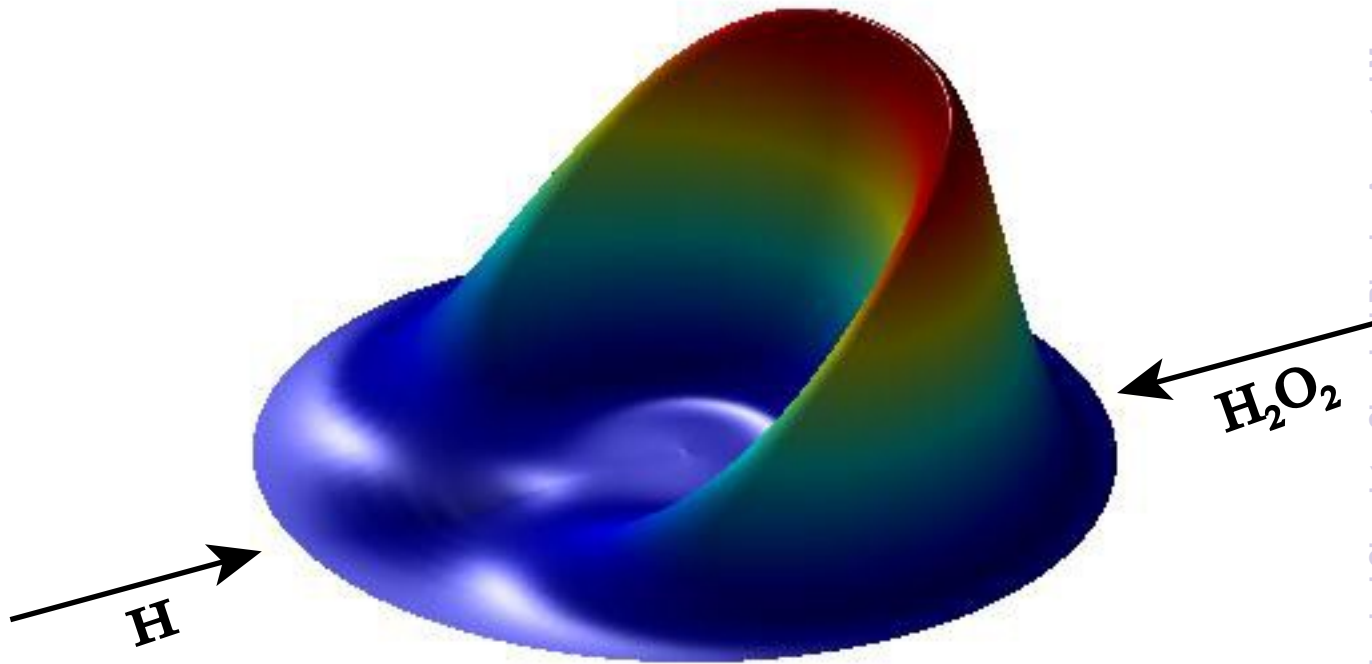


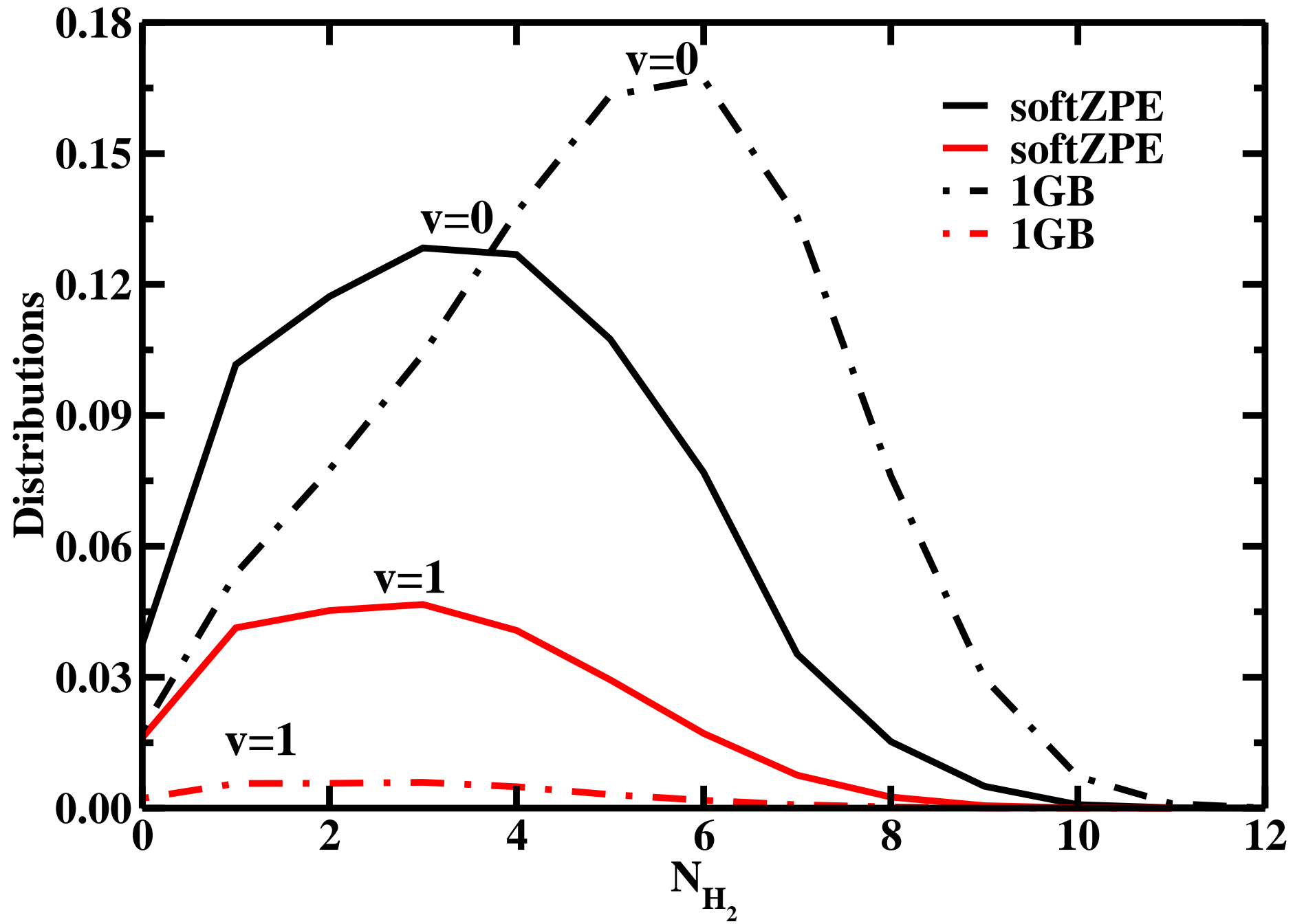


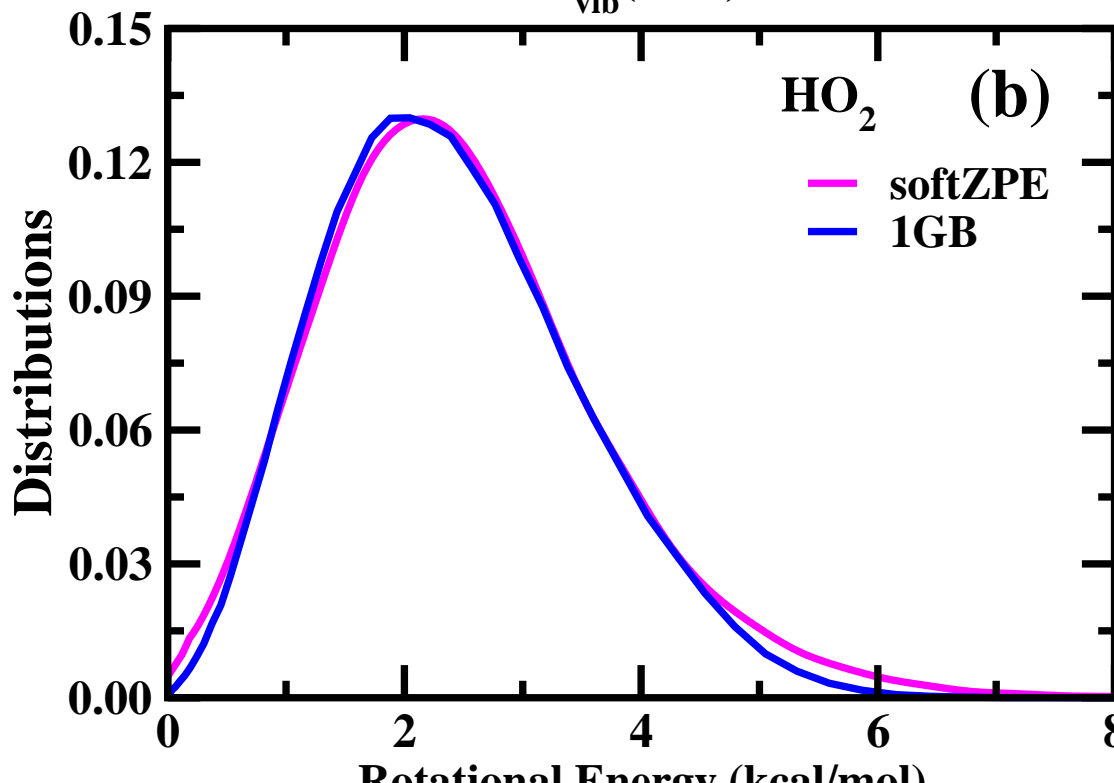
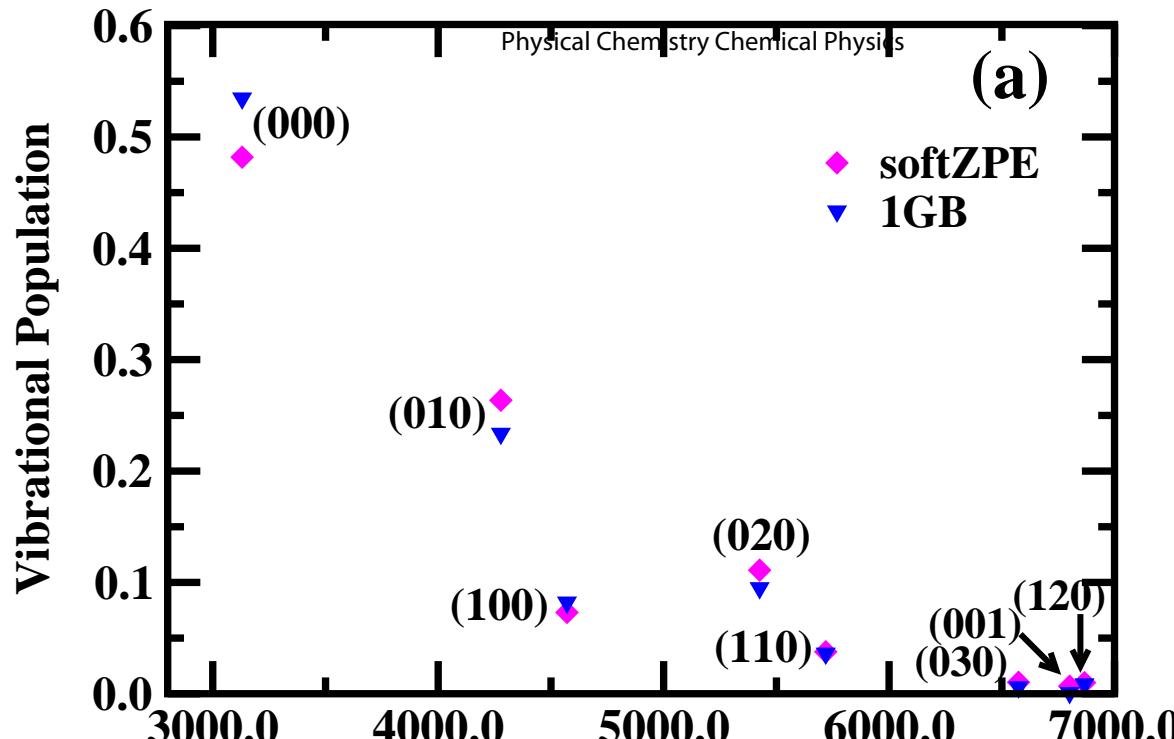


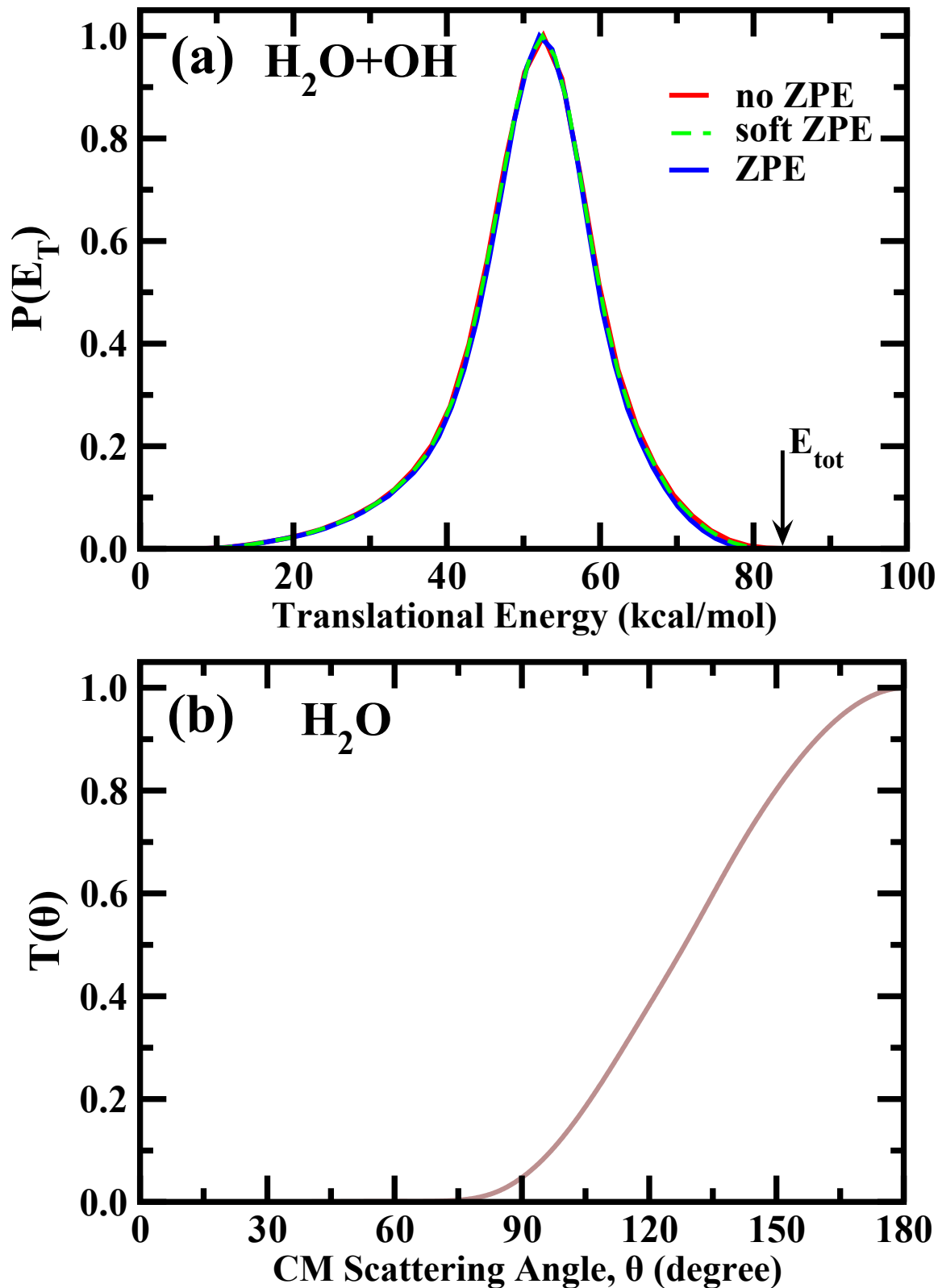


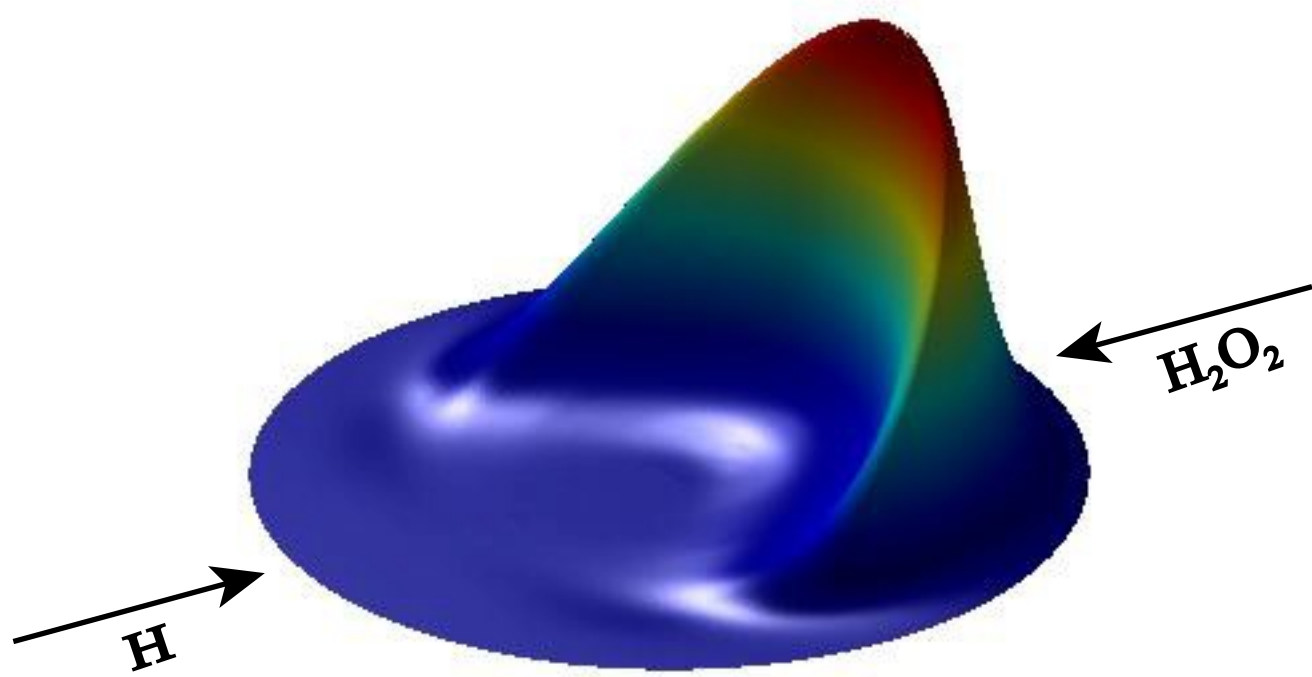


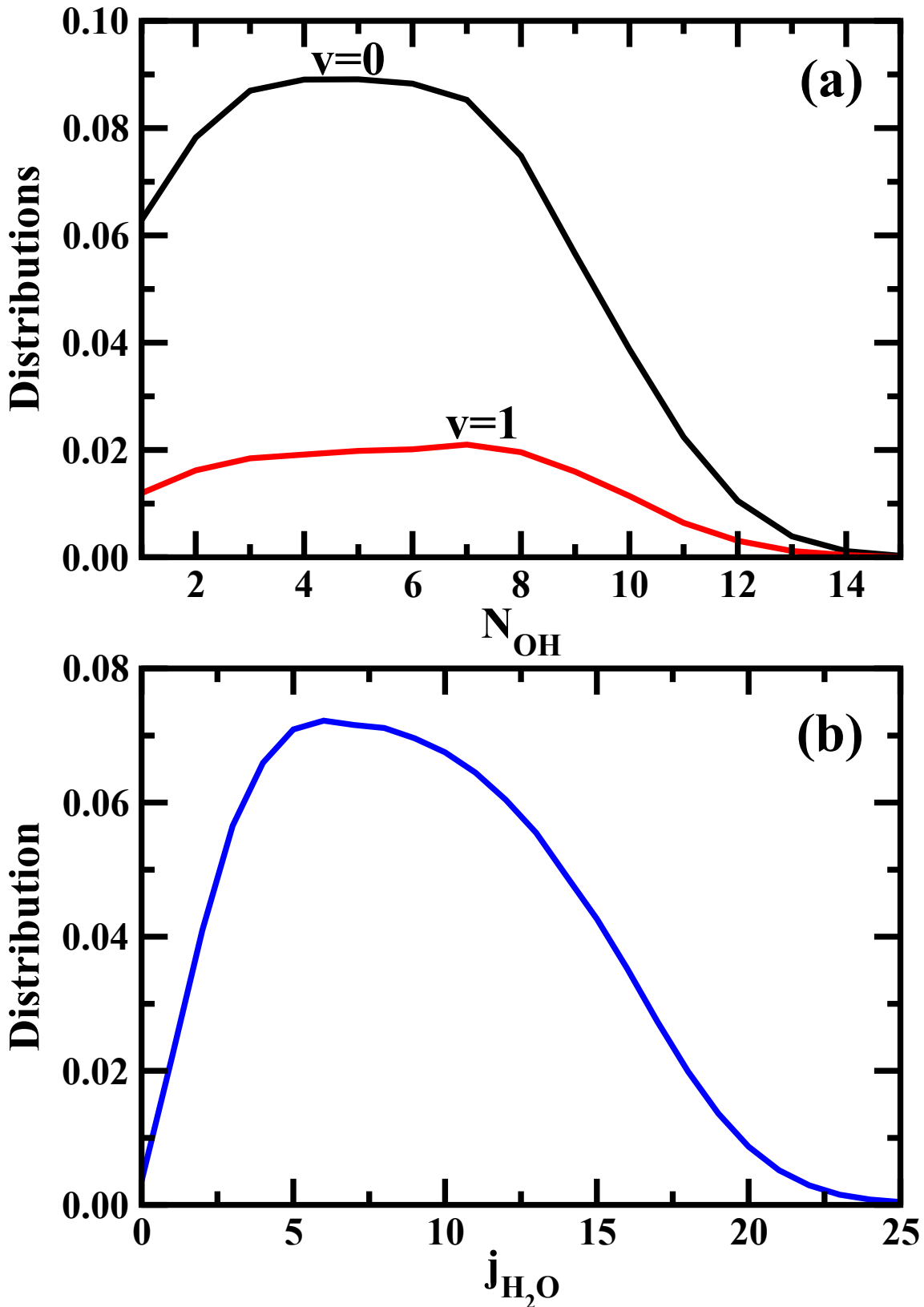


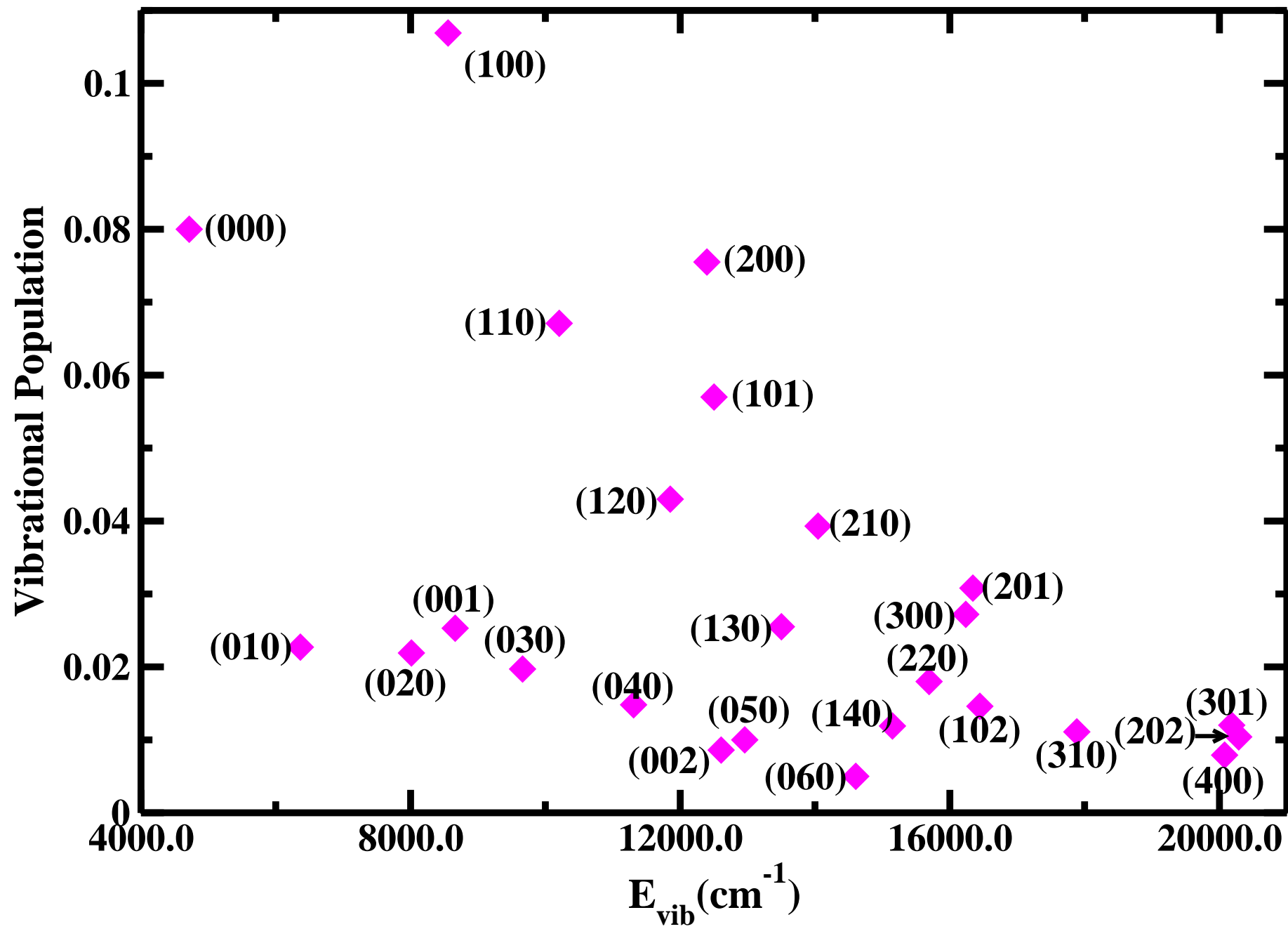












Physical Chemistry Chemical Potential

Page 36 of 36

